The copyright of this thesis vests in the author. No quotation from it or information derived from it is to be published without full acknowledgement of the source. The thesis is to be used for private study or non-commercial research purposes only.

Published by the University of Cape Town (UCT) in terms of the non-exclusive license granted to UCT by the author.

University of Cape Town

Controlling $CoSi_2$ formation temperature by reactive deposition

by

Hind Ali Mohmmed Ahmed

University of Cape Town

A thesis

submitted in fulfilment of the requirements

for the degree of

Masters of Science

in the Department of Physics, Faculty of Science,

University of Cape Town.

May 2008

Supervisor:

Prof. Craig Comrie.

To my parents, sisters and brothers.

University of Cape Town

Keywords

1. Cobalt
2. Silicon
3. Silicides
4. Mono/di-silicide
5. Solid phase reaction
6. Reactive deposition
7. Phase formation
8. Onset temperature formation
9. In situ
10. Real-time RBS
11. Real-time XRD

University of Cape Town

Cobalt-silicide phases : Co_2Si, CoSi and $CoSi_2$.

Abstract

When cobalt is evaporated under ultra high vacuum conditions onto a heated silicon substrate, the reaction between the cobalt and the silicon starts immediately and cobalt silicides are formed directly - a technique referred to as reactive deposition. This procedure was used to grow silicide films over a variety of temperatures ranging between $375 - 550\,^{\circ}\mathrm{C}$. It was found that a disilicide film is formed directly for substrate temperature maintained at $T \geq 550\,^{\circ}\mathrm{C}$, while at $T \leq 475\,^{\circ}\mathrm{C}$ the film is in the form of monosilicide. A mixed mono/di-silicide film is produced when the substrate temperatures are $T = 500\,^{\circ}\mathrm{C}$ and $525\,^{\circ}\mathrm{C}$. Real-time Rutherford Backscattering Spectrometry, in combination with real-time X-Ray Diffraction, was used to investigate how the formation temperature of $CoSi_2$ was effected by the temperature at which the CoSi film was produced by reactive deposition. For the real-time analysis the samples were continuously analysed by Rutherford Backscattering Spectrometry or X-Ray Diffraction while being subjected to a ramped thermal anneal. Real-time X-Ray Diffraction proved to be a very useful method for determining the temperature of onset of the cobalt-silicide phase formation, while real-time Rutherford Backscattering Spectrometry was best able to provide detailed information about the rate of cobalt disilicide formation. It was found that the temperature used to produce CoSi by reactive deposition had a significant effect on the subsequent formation temperature of $CoSi_2$. Analysis of the data shows that the lower the reactive deposition temperature used to form the CoSi film, the higher the subsequent formation temperature of $CoSi_2$. For comparison the rate of formation of cobalt silicides grown from cobalt deposited on silicon substrates at room temperature was also investigated.

University of Cape Town

Declaration

I declare that "*Controlling $CoSi_2$ formation temperature by reactive deposition*" is my own work, that it has not been submitted for any degree or examination in any other university, and that all the sources I have used or quoted have been indicated and acknowledged by complete references.

HIND ALI MOHMMED AHMED *May 2008*

SIGNED: . Signed by candidate

Acknowledgments

I would like to acknowledge my sponsors, the University of Cape Town and the African Institute for Mathematical Sciences (AIMS).

I would also like to thank my supervisor Prof. C.M. Comrie, who prepared the samples at the KU Leuven facility in Belgium and made this project possible. His insight, attention to detail, ideas, comments and help (in particular with my writeup) have been an invaluable.

Most of the analysis was done at iThemba labs. I would like to thank my supervisor Prof. C. M. Comrie again, as well as Prof. C. C. Theron and Dr. R. Nemutudi and the MRG team at iThemba, without whose help this work could not have been completed.

I would also like to thank J. Demeulemeester for performing the real-time XRD measurements of the samples at Gent University.

Furthermore, I am grateful to my friend Timothy[1], for the time he took to read my work and for the numerous fruitful discussions we had about its content. Also, for his assistance at times when LaTeX 2_ε[2] wanted to get out of hand.

I wish to acknowledge my indebtedness to my friend Girma, as his assistance from beginning to end was invaluable.

Finally, I would like to extended my heartfelt gratitude to my loving parents, sisters, brothers and all friends for their support.

University of Cape Town

[1] Thanks again Timothy Kevin Kuria Kamanu (T.K^3)!

[2] LaTeX 2_ε is an extension of LaTeX. LaTeX is a collection of macros for TeX. TeX is a trademark of the American Mathematical Society. The style package *timstyle* was used.

Contents

Title Page i

Keywords iii

Abstract iv

Declaration v

Acknowledgments vi

List of Figures x

List of Tables xvi

Chapter 1: Introduction 1

1.1 Background 1

1.2 Growth Kinetics 2

1.3 Diffusion 3

1.4 Nucleation 5

1.5 Cobalt Silicide System 7

University of Cape Town

Chapter 2: Experimental Techniques **11**

2.1 Procedure 11

2.1.1 Sample preparation 12

2.2 Rutherford Backscattering Technique 13

2.2.1 Kinematic factor (K) 14

2.2.2 Energy loss $(\frac{dE}{dx})$ 15

2.2.3 Differential scattering cross section $(\frac{d\sigma}{d\Omega})$ 17

2.2.4 Characteristics of an RBS spectrum 18

2.2.5 *In situ* real-time RBS 20

2.3 X-Ray Diffraction 25

2.4 Atomic Force Microscopy 27

Chapter 3: Results and Discussion **29**

3.1 RBS analysis 29

3.1.1 Solid phase reaction results 29

3.1.2 Reactive deposition results 34

3.1.3 Co deposited at RT followed by a **450 °C** anneal 43

3.2 Discussion 45

3.3 XRD analysis 46

3.4 Discussion 49

3.5 AFM Analysis 50

3.6 Discussion 52

Chapter 4: Discussion **53**

University of Cape Town

Chapter 5: Conclusions **57**

Appendix A 59

Appendix B 67

Bibliography **68**

University of Cape Town

List of Figures

1.1 Schematic diagram showing that the formation of silicide. M_xSi_y resulted from the diffusion of silicon or metal atoms. 4

1.2 Schematic represetaion of a grain boundary. 4

1.3 (a) Schematic representaion of a new phase AB growing at the interface between two initial phases A and B. (b) The free energy of nucleus as function of its radius showing the surface and the volume contributions (d'Heurle 1988). . 5

1.4 The crystal structure for the different Co silicides (Smeets 2007). 8

2.1 Schematic digram showing the two methods used in the preparation of cobalt silicide film. (a) Solid phase reaction. (b) Reactive deposition. 12

2.2 Schematic layout of a typical backscattering spectrometry system. 14

2.3 Schematic representation of an elastic collision between a projectile of mass M_1 and target atoms of mass M_2. 15

2.4 Illustration of the energy loss for a projectile backscattered at a depth x. 16

2.5 Rutherford backscattering spectrum of CoSi layer on Si. 18

2.6 Real-time RBS setup. 21

2.7 The phase diagram of Au-Si system figure reproduced from Okamoto & Massalski (1983). 21

2.8 The resistance-temperature plot of Au-Si system showing an abrupt rise in resistance at 369 °C. 22

University of Cape Town

2.9 Thermocouple calibration made from the Au-Si and Al-Si systems. 22

2.10 The temperature profile of a ramped anneal. 23

2.11 (a) Display of the four 30-s RBS spectra and (b) composite of 2-min spectra formed by merging the four 30-s spectra in (a) above. 24

2.12 (a) The charge accumulation during the process of annealing. (b) the normalised charge showing the effective current after normalization. 25

2.13 Reflection of X-rays from different atomic planes, illustrating Bragg's law. . . . 26

2.14 Schematic representation of the $\theta - 2\theta$ scan with a linear detector. 27

2.15 The atomic force microscopy (Chen & Waston 1999). 28

2.16 Detection of cantilever by optical beam deflection (Wiesendanger 1994). 28

3.1 (a) Three dimensional plot of RBS spectra obtained during a ramped anneal (2 °C/min) of a 250 Å cobalt film deposited on silicon at room temperature. (b) Contour plot of the data in (a). 30

3.2 Backscattering spectrum showing Co_2Si growth at a thermocouple reading of 372 °C (calibrated temperature of 365 °C). 31

3.3 A backscattering spectrum shows CoSi begins to form at a thermocouple reading of 411 °C before all Co has been consumed (calibrated temperature is 405 °C). 31

3.4 A backscattering spectrum showing complete growth of CoSi at a thermocouple reading of 454 °C (calibrated temperature is 445 °C). 32

3.5 A backscattering spectrum showing the initial growth of $CoSi_2$ at a thermocouple reading of 544 °C (calibrated temperature is 535 °C). 32

3.6 A backscattering spectrum showing a complete growth of $CoSi_2$ at a thermocouple reading of 618 °C (calibrated temperature is 605 °C). 33

3.7 Results of the analysis obtained for Co deposited on Si at room temperature showing the formation of the various cobalt silicides phases. 33

University of Cape Town

3.8 The XRD spectra for the set of samples (as-deposited) that were prepared by reactive deposition at temperatures ranging between 375 – 525 °C (measurements of XRD data performed by J. Demeulemeester at Gent University). 34

3.9 RBS spectra for the set of samples (as-deposited) that were prepared by reactive deposition at temperatures ranging between 375 – 550 °C (an angle of incidence of 10 ° was used). 35

3.10 Contour plot of RBS data obtained during a ramped anneal (2 °C/min) of CoSi film prepared by reactive deposition at 400 °C. 36

3.11 A backscattering spectrum showing CoSi film at a thermocouple reading of 271 °C (calibrated temperature of 267 °C) for the sample made by reactive deposition at 400 °C. 37

3.12 A backscattering spectrum showing the growth of $CoSi_2$ from CoSi by reactive deposition at 400 °C. The $CoSi_2$ starts its formation at a thermocouple reading of 587 °C (calibrated temperature of 575 °C). 37

3.13 A backscattering spectrum of $CoSi_2$ grown from CoSi film produced by reactive deposition at 400 °C showing after all CoSi converted to $CoSi_2$ at a thermocouple reading of 684 °C (calibrated temperature of 670 °C). 38

3.14 Results of the analysis of RBS spectra obtained from the sample produced by reactive deposition at 400 °C. The formation of $CoSi_2$ from CoSi initiated around temperature of 575 °C. 38

3.15 Contour plot of RBS data obtained during a ramped anneal (2 °C/min) of CoSi film prepared by reactive deposition at 450 °C. 39

3.16 A backscattering spectrum showing the onset temperature of $CoSi_2$ at a thermocouple reading of 510 °C (calibrated reading of 500 °C) for the sample prepared by reactive deposition temperature at 450 °C. 39

3.17 A backscattering spectrum showing when all CoSi phase converted to $CoSi_2$ phase at thermocouple reading of 595 °C (calibrated reading of 585 °C) for sample prepared by reactive deposition at 450 °C. 40

University of Cape Town

3.18 Results of the analysis of the RBS spectra obtained from the sample made at 450 °C reactive deposition temperature. The formation of $CoSi_2$ from CoSi began at a temperature of around 500 °C. 40

3.19 Contour plot of RBS data obtained during a ramped anneal (2 °C/min) of CoSi film prepared by reactive deposition at 500 °C. 41

3.20 A backscattering spectrum showing the temperature at which $CoSi_2$ phase began its formation at a thermocouple reading of 476 °C (calibrated reading of 465 °C) for the sample prepared by reactive deposition at 500 °C. 41

3.21 A backscattering spectrum showing when all CoSi phase converted to $CoSi_2$ phase at thermocouple reading of 553 °C (calibrated reading of 540 °C) for the sample prepared by reactive deposition at 500 °C. 42

3.22 Results of the analysis of RBS spectra obtained from the sample prepared by reactive deposition at 500 °C. The formation of $CoSi_2$ from CoSi began at a temperature of around 465 °C. 42

3.23 The onset formation temperatures of $CoSi_2$ produced from CoSi film prepared by reactive deposition at temperatures between 375 – 525 °C. 43

3.24 Contour plot of RBS data obtained during a ramped anneal (2 °C/min) of CoSi film prepared by solid phase reaction when the RT sample annealed to 450 °C. . 43

3.25 A backscattering spectrum showing when $CoSi_2$ is observed to begin its formation at a thermocouple reading of 544 °C (calibrated reading of 535 °C) for sample deposited at RT followed by 450 °C anneal. 44

3.26 A backscattering spectrum showing a complete growth of $CoSi_2$ at a thermocouple reading of 587 °C (calibrated reading of 575 °C). 44

3.27 Results of the analysis of the RBS spectra for the sample deposited at RT followed by 450 °C anneal. The formation of $CoSi_2$ from CoSi initiated at a temperature of 535 °C. 45

3.28 Temperature of onset of the formation of $CoSi_2$ from CoSi grown by reactive deposition at a temperature ranging from 375 °C to 525 °C. 46

University of Cape Town

3.29 (a) The XRD data obtained during the ramp annealing at 1 °C/s of Co deposited at RT. (b) the XRD data for the same sample which had been pre-annealed at 450 °C to convert it to the CoSi phase. In both panels the formation of $CoSi_2$ phase was observed to appear at a temperature of 560 °C (measurements of XRD data performed by J. Demeulemeester at Gent University). 47

3.30 The XRD data obtained during the ramp annealing of Co reactive deposited at (a) 400 °C, (b) at 450 °C and (c) at 500 °C. The figure shows the formation of $CoSi_2$ phase, which begins at a lower temperature when the sample is prepared at a higher reactive deposition temperature (measurements of XRD data performed by J. Demeulemeester at Gent University). 48

3.31 Temperature of onset of the formation of $CoSi_2$ from CoSi films grown by reactive deposition at temperature ranging from 375 °C to 500 °C. 49

3.32 3-D AFM images of CoSi film prepared by reactive deposition at (a) 400 °C, (b) 450 °C and (c) 500 °C. 50

3.33 3-D AFM images of $CoSi_2$ formed after ramped anneal of CoSi prepared at (a) 400 °C, (b) 450 °C and (c) 500 °C reactive deposition temperatures. 51

4.1 Graph displaying the onset temperature formation of $CoSi_2$ phase from CoSi-film prepared by reactive deposition at different temperatures (375 – 525 °C). The graph also shows the temperature formation of $CoSi_2$ prepared by solid phase reaction. 54

A1 Contour plot of RBS data obtained during a ramped anneal (2 °C/min) of CoSi film prepared by reactive deposition at 375 °C. 59

A2 Results of the analysis of RBS spectra obtained form CoSi prepared by reactive deposition at 375 °C. The formation of $CoSi_2$ from CoSi initiated at calibrated temperature of 585 °C. 60

A3 Contour plot of RBS data obtained during a ramped anneal (2 °C/min) of CoSi film prepared by reactive deposition at 455 °C. 61

University of Cape Town

A4 Results of the analysis of RBS spectra obtained form CoSi prepared by reactive deposition at 425 °C. The formation of $CoSi_2$ from CoSi started at calibrated temperature of 560 °C. 62

A5 Contour plot of RBS data obtained during a ramped anneal (2 °C/min) of CoSi film prepared by reactive deposition at 475 °C. 63

A6 Results of the analysis of RBS spectra obtained form CoSi prepared by reactive deposition at 475 °C. The formation of $CoSi_2$ from CoSi started at calibrated temperature of 485 °C. 64

A7 Contour plot of RBS data obtained during a ramped anneal (2 °C/min) of CoSi film prepared by reactive deposition at 525 °C. 65

A8 Results of the analysis of RBS spectra obtained form CoSi prepared by reactive deposition at 525 °C. The formation of $CoSi_2$ from CoSi initiated at calibrated temperature of 450 °C. 66

B1 The XRD data obtained during the ramp annealing of CoSi prepared by reactive deposition at 375 °C (measurements of XRD data performed by J. Demeulemeester at Gent University). 67

B2 The XRD data obtained during the ramp annealing of CoSi prepared by reactive deposition at 425 °C (measurements of XRD data performed by J. Demeulemeester at Gent University). 68

B3 The XRD data obtained during the ramp annealing of CoSi prepared by reactive deposition at 475 °C (measurements of XRD data performed by J. Demeulemeester at Gent University). 68

B4 The XRD data obtained during the ramp annealing of CoSi prepared by reactive deposition at 525 °C (measurements of XRD data performed by J. Demeulemeester at Gent University). 69

University of Cape Town

List of Tables

1.1 Table showing formation sequence, crystal structure and formation temperature of cobalt silicides. Data taken from Lau et al. (1978) and Ottaviani et al. (1987). 7

University of Cape Town

Chapter 1

Introduction

1.1 Background

A silicide is a compound of silicon and another metal from the periodic table. Over the past few decades, a wide range of transition metals such as Ti, Ni, Pd, Pt, Fe, Cr, Co and suchlike have been extensively investigated (Comrie & Egan 1988, Comrie et al. 1988, Falepin et al. 2001, Jeon et al. 2002, Theron 1994, Wandt et al. 1990, Zingu et al. 1983) due to their potential use in microelectronic devices. They have been used as ohmic contacts, Schottky barrier contacts, gate electrodes, local interconnects and diffusion barriers (Chen 2005).

Metal silicide thin films are formed by a reaction between a silicon substrate and a deposited metal layer, usually as a result of thermal treatment. However, alternative methods such as sputtering (Chamirian et al. 2002, Naidoo et al. 1993) or co-evaporation (d'Heurle et al. 1985) are also employed to form these compounds. Reaction between the metal and the silicon substrate can also be achieved by depositing the metal onto a heated substrate in reactive deposition (Comrie et al. 2007, Reader et al. 1993, Vantomme et al. 1996), or reactive deposition epitaxy (Lim et al. 2006). Moreover, silicides may also be produced by ion beam mixing (Mogul et al. 1993) or by laser irradiation (Comrie et al. 2004, Falepin et al. 2003).

Amongst the metal silicides, epitaxial silicides have received considerable attention due to their thermal stability, lower electrical resistivity, and more importantly the potential to epitaxially overgrow the silicide layer with more silicon (Nicolet & Lau 1993). These features could po-

University of Cape Town

tentially open the way to the creation of new classes of devices based on semiconductor-metal-semiconductor multilayer structures. One of the most studied of the epitaxial silicides is $CoSi_2$, which has replaced titanium in silicon technology to form highly conductive narrow lines on the gate stack of modern metal-oxide-semiconductor devices (Alberti et al. 2003, Lauwers et al. 2002).

$CoSi_2$ has a cubic fluorite lattice structure and a mismatch on silicon of 1.2%. It also has one of the lowest electrical resistivities ($\approx 14\ \mu\Omega$cm) at room temperature among all metal silicides (Tung 1992). Most of the epitaxial work (Bulle-Lieuwma 1993, Comrie & Hoffman 1993, Tung 1992) undertaken thus far has focused on $CoSi_2$/Si<111>, as easier to grow $CoSi_2$ films with a high epitaxial quality on Si<111> substrates compared to Si<100>, which has been found to be difficult (Yalisove et al. 1989). However, it has become clear that the growth of epitaxial $CoSi_2$ on Si<100> substrates could have a greater technological impact than on Si<111>. As such, a great deal of efort has been devoted to growing high-quality films on Si<100> substrates (Jimenez et al. 1990, Kluth et al. 2000, Reader et al. 1993, Vantomme et al. 1996, 1995, 1994).

In recent years the microelectronic industry has focussed on CoNi-silicides in the belief that these can replace $CoSi_2$ as a contact material for source/drain areas in complementary metal-oxide-semiconductor (CMOS) technologies (Alberti et al. 2003, Lauwers et al. 2002). However, the use of CoNi-silicides is becoming troublesome, as they exhibit an increase in resistance as the gate length decreases below 40 nm (Kittl et al. 2003). At present, NiSi seems to be the most promising candidate to replace $CoSi_2$ within the microelectronic industry (Lavoie et al. 2003).

University of Cape Town

1.2 Growth Kinetics

There are generally two main types of growth, that lead to silicide formation. The first type results in the formation of laterally uniform silicide layers with well defined kinetics and temperature dependence, while the second type produces non-uniform growth with critical temperature dependence (d'Heurle & Gas 1986, Nicolet & Lau 1993).

In the first type, the reaction takes place over a relatively wide temperature ranges and growth proceeds with lateral uniformity and relatively sharp interfaces. In terms of this type, the growth

rate may follow a ($\sqrt{t}$) time dependence indicating a diffusion controlled reaction, or it may be linear with time, which is indicates that is reaction controlled, if the rate limited by the interfacial reaction. NiSi, Ni_2Si, PtSi and Pt_2Si are examples that follow a diffusion controlled reaction (Nicolet & Lau 1993), while $MoSi_2$, VSi_2, $CrSi_2$ and $TiSi_2$ are reported to be reaction controlled (d'Heurle & Gas 1986).

In the second type of growth (referred to as nucleation controlled), growth only takes place after a critical temperature has been reached. This critical temperature is generally well defined, and is typically within a range of 10 to 30 °C (Nicolet & Lau 1993). Often the critical temperature is high, and once nucleation occurs the growth rate is extremely rapid, making it difficult to analyse. This kind of reaction leads to columnar growth which results in laterally nonuniform features (Nicolet & Lau 1993). Examples of silicide with nucleation controlled kinetics are: Rh_4Si_5, $NiSi_2$ and $IrSi_3$ (see d'Heurle & Gas 1986, for the details). $CoSi_2$ has also been reported by Appelbaum, Knoell & Muraka (1985) to follow nucleation controlled kinetics where the reaction occurs in four stages: (a) nucleation of the $CoSi_2$ phase at the grain boundary triple points, (b) lateral growth from the nucleation sites to form a continuous layer on the silicon substrate, (c) growth in thickness by diffusion through the $CoSi_2$ layer, and finally (d) a lateral epitaxial growth by elimination of the grain boundaries.

University of Cape Town

1.3 Diffusion

To form a compound at the interface between two adjoining elemental solids, there must be relative motion of atoms past each other. The mechanism of movement is referred to as diffusion. An understanding of diffusion mechanisms is important in order to comprehend changes that occur in solid during the annealing process. During silicides growth atoms may diffuse from the silicon substrate or from the metal as indicated by arrows in Figure 1.1.

Metal silicides are formed at the interface in both cases. However, it is difficult to tell the direction in which atoms diffuse during solid state reaction unless a marker technique (Comrie 1996, Mcleod et al. 1992) is employed.

Generally, there are different ways in which atoms can diffuse in a lattice composed of an

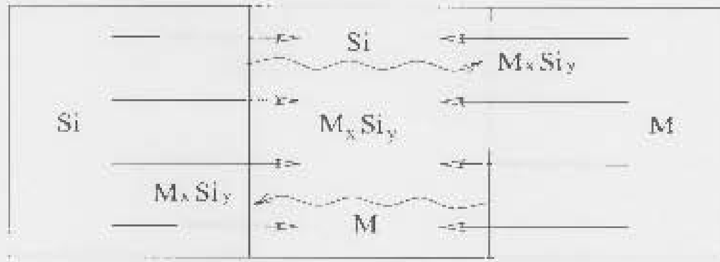

Figure 1.1: Schematic diagram showing that the formation of silicide, M_xSi_y resulted from the diffusion of silicon or metal atoms.

ordered matrix. The diffusant may move substitutionally by occupying lattice sites, or interstitially by transferring through a sub-lattice of vacant interstitial sites between the main matrix atoms (Christain 1975). However, different mechanisms such as vacancy and interchange mechanisms have also been postulated with respect to atom movement substitutionally (Glicksman 2000, Walton 1982).

Another possible diffusion mechanism is grain boundary diffusion. Figure 1.2 shows a schematic representation of grain boundary. The term grain boundary diffusion is refers to atomic movements occurring in the interfacial region separating two grains. This region provides high mobility routes for atomic migration relative to lattice diffusion. Therefore, the diffusion through highly defected areas such as grain boundaries often requires a lower activation energy compared to that for lattice diffusion (Smoluchowski 1952). This diffusion mechanism is commonly observed in thin films due to their high density of grains.

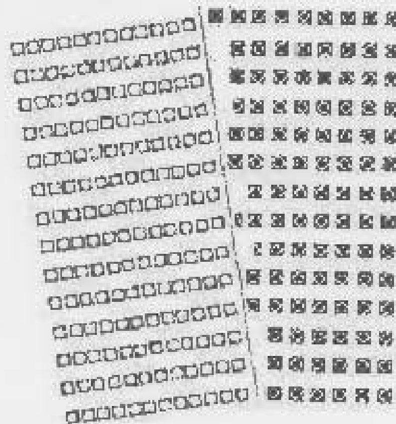

Figure 1.2: Schematic represetaion of a grain boundary.

University of Cape Town

1.4 Nucleation

The following section provides an overview of the classical theory of nucleation as described in the literature by d'Heurle (1988) who has written an excellent review on nucleation in silicide formation. When a new phase AB grows between two phases A and B [see Figure 1.3(a)], the driving force of the formation of AB from pure A and B for this reaction is ΔG (Gibbs energy). However, the formation of AB involves the creation of two new interfaces, A/AB and AB/B instead of a single A/B interface, therefore an increase of the interfacial energy $\Delta\sigma$ results. There is therefore a decrease in free energy by transformation of a volume A and B into nucleus AB with radius r which results in an energy gain $\Delta G_V \sim r^3\Delta G$. On the other hand, the additional interfaces result in an increase in surface energy, $\Delta\sigma \sim r^2\sigma$. The total free energy of a nucleus with radius r is then given by:

$$\Delta G_N(r) = ar^2(\Delta\sigma) - br^3\Delta G. \tag{1.1}$$

where a and b are geometrical terms that take into account the shape of the nucleus. The relationship between the free energy of nucleus and its radius r is shown in Figure 1.3(b).

University of Cape Town

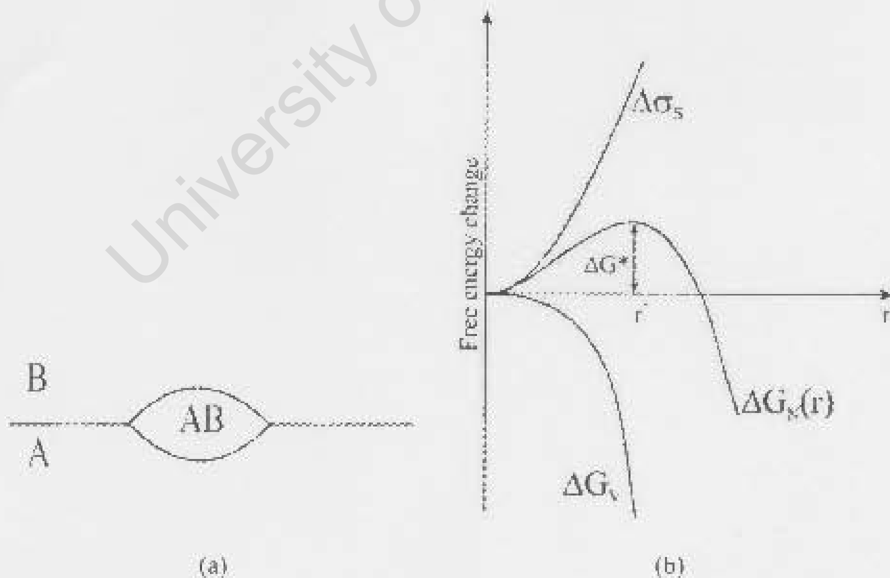

Figure 1.3: (a) Schematic representaion of a new phase AB growing at the interface between two initial phases A and B. (b) The free energy of nucleus as function of its radius showing the surface and the volume contributions (d'Heurle 1988).

For a critical radius r^*, the change in free energy has a maximum value ΔG^* as seen in Figure 1.3(b). Nuclei with a radius smaller than r^* exists in some equilibrium concentration but are not able to grow. In contrast, nuclei with a radius bigger that r^* are able to grow. The free energy of a nucleus with radius r^*, ΔG^* can therefore be calculated as follows:

$$r^* \approx \frac{\sigma}{\Delta G}, \tag{1.2}$$

$$\Delta G^* \approx \frac{\sigma^3}{(\Delta G)^2} = \frac{\sigma^3}{(\Delta H - T\Delta S)^2}. \tag{1.3}$$

ΔG^* can be regarded as the activation energy for the nucleation of the new phase. The rate of nucleation ρ^* will be proportional to the concentration of critical nuclei and the rate at which such nuclei grow. The rate of nucleation ρ^* is given by the product of the concentration of nuclei of critical size ρ^* and some diffusion terms Q, considering the local atomic rearrangement needs to form the nucleus:

$$\rho^* \approx exp(-\Delta G^*/KT)exp(-Q/KT). \tag{1.4}$$

It is clear from (1.3) that the nucleation will only be rate limiting if ΔH is small. Typically, this is not the case for the first phase that forms between a metal and Si. The nucleation effects are therefore only required for the formation of the second or third phases.

It has been reported (Appelbaum et al. 1985) that the formation of $CoSi_2$ is also nucleation controlled. Because of the small difference in formation enthalpy between CoSi and $CoSi_2$, it may be expected that nucleation is a rate controlling process. However, the nucleation temperature of $CoSi_2$ is low (around 550 °C), and once a stable nucleus is formed slow diffusional kinetics are still observed. If the formation of $CoSi_2$ can be achieved in direct reaction between Co and Si, a very low activation energy for nucleation will result, as ΔH for this reaction is much larger (Detavernier et al. 2000). More information about nucleation can be found in Laurila & Molarius (2003), Venables et al. (1984) and Christain (1975).

University of Cape Town

1.5 Cobalt Silicide System

In the cobalt silicide system in which thin layers of cobalt are deposited onto a silicon substrate, Si is observed (at a temperature of 300 °C) to diffuse through the Co layer via the grain boundary of the Co layer, and accumulated at the sample surface (Lau et al. 1978). The metal rich silicide, Co_2Si, is reported (Cahoon et al. 1984, Colgan et al. 1995, Gurp & Langereis 1975, Theron 1997) as the first phase to grow. However, Lau, Mayer & Tu (1978) have reported that Co_2Si and CoSi initially grow side-by-side, and that Co_2Si transforms to CoSi once all the Co is consumed. Based on thermodynamic grounds, the CoSi phase should be the first to form as it constitutes the silicides with the most negative Gibbs energy of formation in the cobalt silicide system. On the other hand it is found that the activation energy of growth for the CoSi phase (1.9 eV) is considerably higher than that of the Co_2Si phase (1.5 eV) (Lau et al. 1978). It is therefore possible, for kinetic reasons, that Co_2Si grows first and is followed by a simultaneous growth of Co_2Si and CoSi. The last phase in the cobalt silicides system $CoSi_2$, does not grow until the temperature rises to 550 °C (Ottaviani et al. 1987). The phase formation can be summarised as follows:

Similar to other metal silicides, these cobalt silicides have unique crystal structures. Table 1.1 summarises the phase sequences, crystal structures and temperatures at which these silicide phases begin to form, as reported in the literature reviewed. Figure 1.4 presents the crystal structure of the cobalt silicides.

Phase sequence	**Silicide**	**Crystal structure**	**formation temperature**
First phase	Co_2Si	Orthorhombic, $PbCl_2$	≈ 350 °C
Second phase	CoSi	Cubic, $\epsilon - FeSi$	≈ 375 °C
Final phase	$CoSi_2$	Cubic, CaF_2	≈ 550 °C

Table 1.1: Table showing formation sequence, crystal structure and formation temperature of cobalt silicides. Data taken from Lau et al. (1978) and Ottaviani et al. (1987).

It has been reported (Comrie & Mcleod 1992, Smeets 2007, Van et al. 1978) that cobalt is the dominant moving species during first phase formation, while silicon is that during the second

University of Cape Town

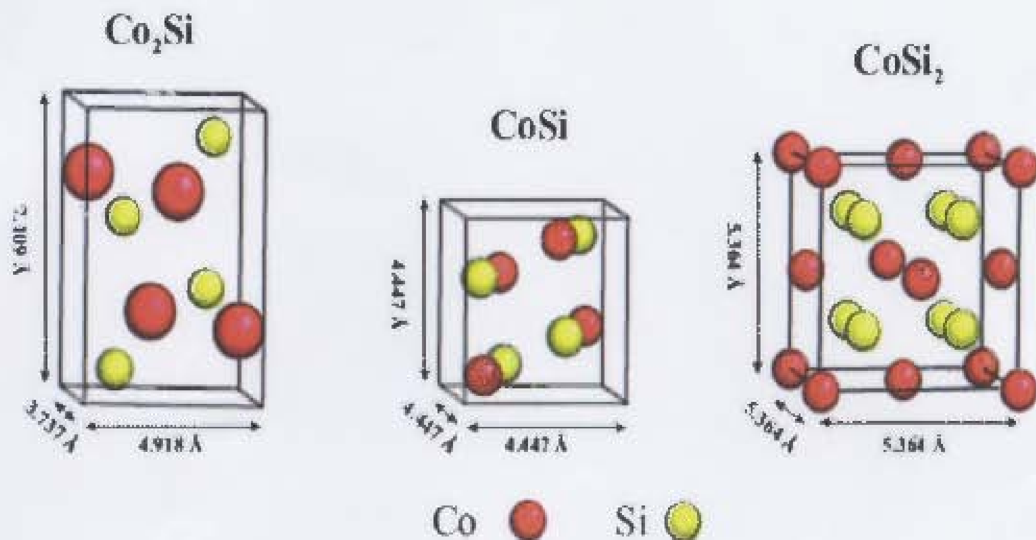

Figure 1.4: The crystal structure for the different Co silicides (Smeets 2007).

University of Cape Town

phase (Comrie & Mcleod 1992, Pretorius et al. 1989, Smeets 2007, Van et al. 1978). The thicknesses in both Co_2Si and CoSi are found to be proportional to the square root time, which suggests that the growth process is diffusion controlled (Lau et al. 1978). The growth of Co_2Si was proposed to be via a grain boundary diffusion mechanism (Smeets 2007), and the same has been found for CoSi (Pretorius et al. 1989, Smeets 2007).

For the $CoSi_2$ phase, Co has been reported (d'Heurle & Petersson 1985, Lien, Artur & Nicolet 1984) to be the sole moving species based on a Xe marker. Comrie (1996) showed that the Xe marker is most likely to be in error and while his results indicate that both species differ during growth, he reported that Si is the dominant moving species during disilicide formation. However, van Dal et al. (2001), reported that Co and Si have comparable diffusivities in the formation of the $CoSi_2$ phase in a temperature range of 1048 – 1217 °C.

Like its diffusion moving species, the kinetics growth of $CoSi_2$ is also complicated due to a combination of nucleation and diffusion effects. For annealing temperatures higher than nucleation temperature, the thickness of the layer is found to be proportional to the square root of time, indicating that the growth of $CoSi_2$ is diffusion controlled (Pretorius et al. 1985). It was found (Lien, Nicolet & Lau 1984) that the nucleation temperature is lowered when $CoSi_2$ is grown on amorphous Si, and the $CoSi_2$ is therefore grown layer-by-layer. Appelbaum et al.

(1985) concluded that the reaction CoSi + Si ⇒ $CoSi_2$ is nucleation controlled, occurring in four stages as discussed earlier (page 3).

As mentioned in section 1.1, there are many techniques used to form silicides. Only two of these were however used to grow cobalt silicides in this investigation. The first technique, solid phase reaction, entails the deposition of a cobalt layer on a Si<100> substrate at room temperature. The reaction of the cobalt with the silicon substrate during the subsequent annealling results in growth of various cobalt silicide phases. Thermodynamics and kinetics play an important role during the growth. As such, silicide reaction sequences have been discussed thoroughly in terms of simple thermodynamic rules (Molinder 1956).

The second technique used to grow cobalt silicides in this investigation is referred to as reactive deposition. In terms of this technique, silicide formation is achieved by depositing of cobalt onto a heated silicon substrate which causes immediate reaction. The silicide phase formed in this way can be controlled by the deposition rate of the cobalt atoms and/or the temperature at which the substrate is held. The cobalt supply to growth interface can be controlled by its individual deposition rate, while the supply of silicon to the reaction interface can be controlled by the temperature of the substrate. Being able to control each rate independently of the other makes it much easier to unravel the processes involved in binary silicide formation.

There has been some research into epitaxial $CoSi_2$, formed by this technique (i.e. reactive deposition). Vantomme et al. (1996) used a cobalt deposition rate of 0.07 to 0.28 Å/s and kept the substrates at a temperature ranging from 500 − 650 °C, at which the cobalt deposition was performed. The results of their experiments showed how growth parameters such as the deposition rate and substrate temperature are crucial in determining the epitaxial nature of silicides. According to Vantomme et al. (1996), a good $CoSi_2$/Si alignment is only achieved when a low deposition rate (0.1 Å/s or less) is used combined with a relatively high substrate temperature (∼ 600 °C or higher) during the deposition. In essence their model can be summarised by the requirement to limit the Co flux to a low enough value in order to prevent Co-rich silicide formation.

Reader et al. (1993) also found that the rate of metal supply to a hot Si substrate determines whether epitaxial or polycrystalline $CoSi_2$ is produced during the reaction. In their experiments, Co was deposited at rate of 0.01 nm/s onto heated Si substrates at 500 °C and 600 °C. Their

University of Cape Town

results showed that the deposition of Co onto a Si substrate at 500 °C leads to the formation of polycrystalline $CoSi_2$, while deposition at the same rate onto a substrate at 600 °C leads to the formation of epitaxial disilicide.

Since reactive deposition can produce $CoSi_2$ films of superior epitaxy quality it raises the question of whether it possible to grow CoSi films by reactive deposition, and if so, how these compare to those grown by solid phase reaction. To the best of our knowledge, there has not been any detailed investigation undertaken into mono-silicide formation by reactive deposition. As one of the most distinctive features of the Co/Si system is the nucleation controlled formation of the $CoSi_2$ phase, one method of checking for differences in the CoSi films grown by the two techniques is to investigate whether reactive deposition has any effect on the nucleation temperature of the $CoSi_2$ phase. Since such an investigation is best carried out *in situ* during a thermal anneal it was decided to use a combination of real-time Rutherford Backscattering Spectrometry and real-time X-Ray Diffraction, as this would also allow for a comparison to be made between the two techniques. Hopefully our results address the questions posed above.

This work is divided into five chapters. The next chapter provides details of the sample preparation and describes the analytical techniques used in this study. In particular, the principle of Rutherford Backscattering Spectrometry, X-Ray Diffraction and Atomic Force Microscopy are discussed. The experimental results obtained in the investigation are reported in chapter three. These results are discussed in chapter four and a general conclusion is presented in chapter five.

University of Cape Town

Chapter 2

Experimental Techniques

In this investigation three analytical tools, namely the Rutherford Backscattering Spectrometry (RBS), X-Ray Diffraction (XRD) and Atomic Force Microscopy (AFM) were used. The main experimental technique used was RBS, while XRD and AFM were less extensively utilised. In this second chapter, a detailed description of sample preparation will be presented and the theoretical basis for the aforementioned experimental techniques will be discussed.

2.1 Procedure

As mentioned in chapter one, only two methods were used to prepare cobalt silicides: solid phase reaction and reactive deposition. Figure 2.1 illustrates these two techniques.

In solid phase reaction, Figure 2.1(a), a cobalt film is deposited by e-beam evaporation onto a Si substrate maintained at room temperature. The cobalt film is then heated to supply the necessary energy for the formation of the silicide.

In reactive deposition, Figure 2.1(b), the immediate reaction between the cobalt and the silicon during deposition of the film is achieved by depositing cobalt onto a heated silicon substrate. The silicide phase formation is controlled by the deposition rate of the cobalt atoms together with the temperature of the silicon substrate.

University of Cape Town

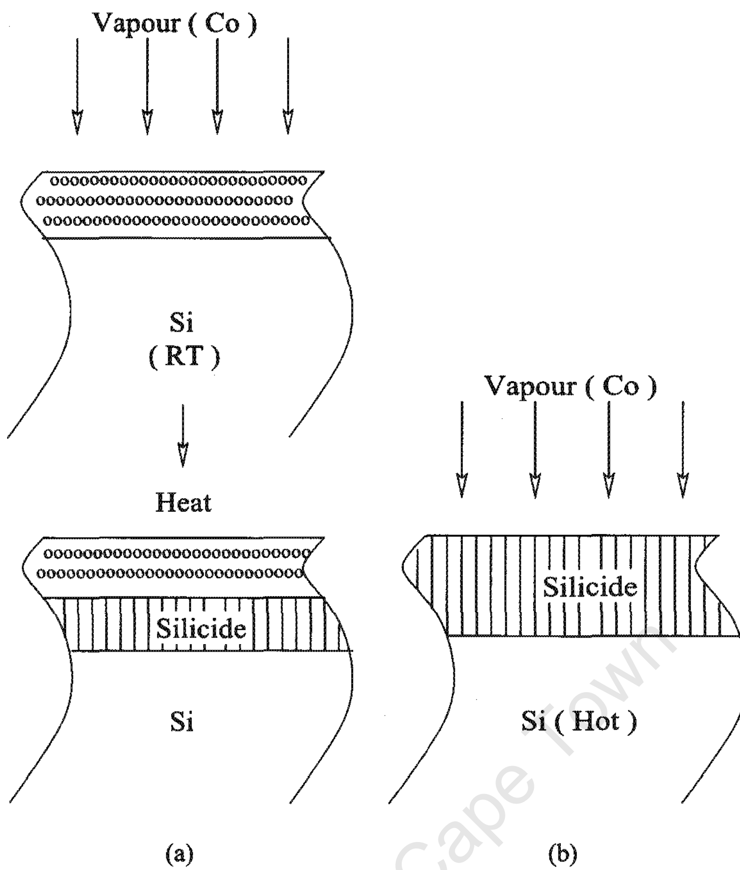

Figure 2.1: Schematic digram showing the two methods used in the preparation of cobalt silicide film. (a) Solid phase reaction. (b) Reactive deposition.

University of Cape Town

2.1.1 Sample preparation

The samples used in this investigation were prepared by C.M. Comrie at the KU Leuven facility in Belgium. As native silicon-oxide film and other contaminants are almost always present at the surface of a Si substrate, these need to be removed before the deposition of the metal film. In this study two inch silicon wafers were therefore cleaned by an RCA to remove any organic residues from the sample surface. The wafers were then dipped in a diluted 2% hydrofloride acid solution (HF) for two minutes to remove any oxide film and to terminate the dangling Si bonds with hydrogen. After cleaning the silicon wafer was mounted on a solid molybdenum block, introduced into a load-lock and then transferred into a UHV molecular beam epitaxy (MBE) chamber.

For samples prepared by solid phase reaction, a 250 Å cobalt film was deposited at a rate of

0.125 Å/s on silicon substrates held at room temperature. The pressure during deposition was kept below 1×10^{-10} torr.

The same cleaning procedure, vacuum condition and deposition rate were used for samples prepared by reactive deposition. However, during the reactive depositions the substrates were kept fixed at a temperature high enough to induce silicides phase formation. The temperature used in the investigation ranged between $375 - 550\,^{\circ}$C. The samples were then allowed to cool to $< 80\,^{\circ}$C before removing them from the MBE chamber.

All the samples were analysed using RBS as well as by XRD. Atomic force microscopy analysis was also carried out on selected samples.

2.2 Rutherford Backscattering Technique

University of Cape Town

The first examples of backscattering was by Geiger and Marsden in 1909 (Geiger & Marsden 1909), whose effects were later explained by the Rutherford atomic model in 1911 (Rutherford 1911). Since then RBS has becomes an important and commonly applied technique for the study of thin films. The technique has the advantage of allowing analysis to be made non-destructively and reliably (Ziegler 1975). RBS is a fast and direct method for obtaining element depth profiles in solids (Chu et al. 1973, Ziegler 1975). The RBS technique is simple in nature. The schematic layout of an RBS experiment is illustrated in Figure 2.2. A beam of monoenergetic (in the MeV range) collimated alpha particles impinge on a target and a fraction of the backscattered the particles is analysed with a silicon barrier detector placed at a fixed scattering angle. The scattered particles which strike the detector generate an electrical signal which is amplified and processed with rapid analog and digital electronics. The data collected in the final stage has the form of a digitised spectrum (Chu et al. 1978). RBS basically relies on the following three physical concepts:

1. the kinematic factor K;
2. the energy loss of a particle $(\frac{dE}{dx})$;
3. and the differential scattering cross-section $(\frac{d\sigma}{d\Omega})$.

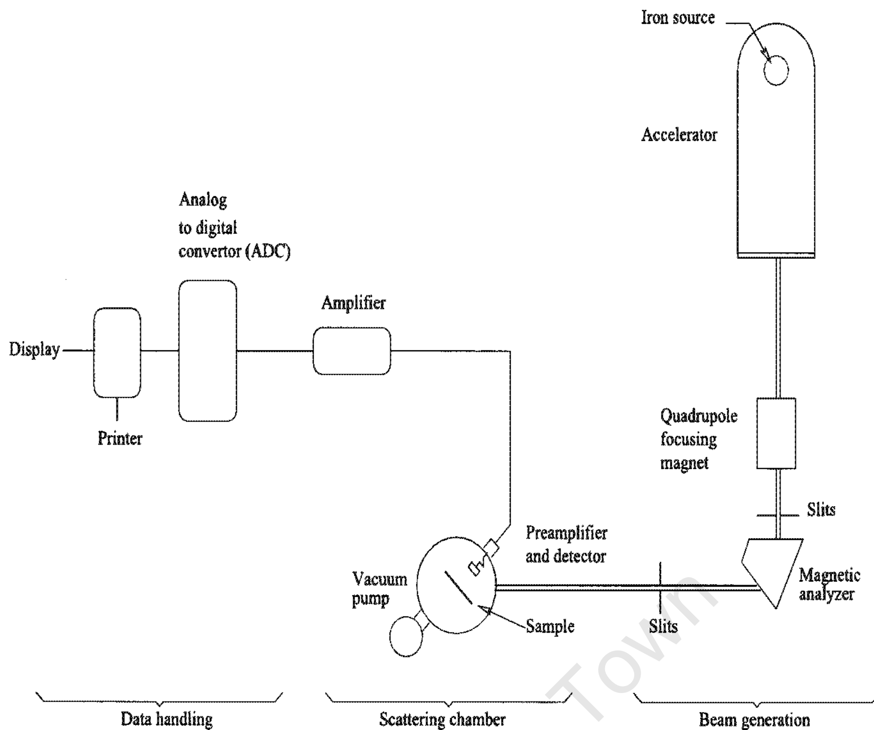

Figure 2.2: Schematic layout of a typical backscattering spectrometry system.

University of Cape Town

2.2.1 Kinematic factor (K)

When a beam of alpha particles collides with a stationary target atom the incident particles may be scattered by the target atoms. Providing the energy of the incident particles is very much larger than the binding energy of atoms in the target, but below the energy at which nuclear reactions will occur, the interaction can be treated as a simple elastic collision which obey the laws of conservation of energy and momentum. Figure 2.3 illustrates a collision between an incident energetic particle with mass M_1, velocity v_0, and energy E_0 and a target atom with mass M_2. During the collision, there will be a transfer of energy from the moving particle to the stationary target atom, leading to final velocities and energies v_1, E_1 and v_2, E_2 respectively. The reduction energy of the scattered incident particles depends on the masses of incident and target atoms. The ratio of the projectile energies, E_0 and E_1 is defined as kinematic factor K.

$$K = \frac{E_1}{E_0} \tag{2.1}$$

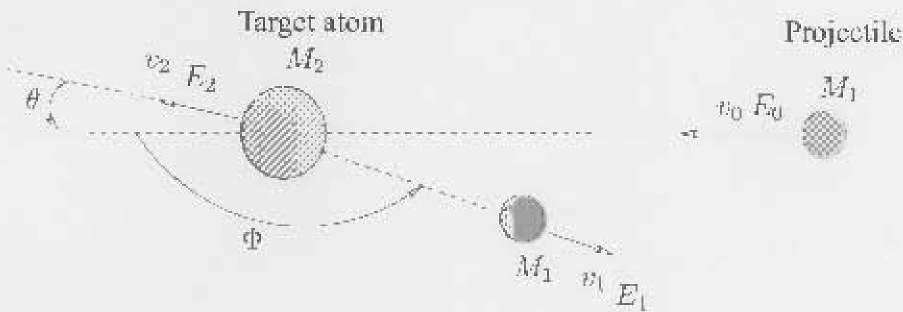

Figure 2.3: Schematic representation of an elastic collision between a projectile of mass M_1 and target atoms of mass M_2.

Considering the collision to be elastic, energy and momentum are conserved. From this, the ratio of the projectile energies can be calculated for $M_1 < M_2$ as

$$K = \frac{E_1}{E_0} = \left[\frac{(M_2^2 - M_1^2 \sin^2\theta)^{\frac{1}{2}} + M_1\cos\theta}{M_1 + M_2}\right]^2 \tag{2.2}$$

Equation 2.2 shows the dependence of the energy of the backscattered particle on the target mass and the scattering angle θ. However during a measurement the kinematic factor K only depends on the mass of the target atom M_2 since the detector angle θ and the mass of the projectile M_1 is constant. If the energy of the projectile E_0 and its mass M_1 are known, one can determine M_2 (i.e. the mass of the atoms from which they are scattered), by measuring the energy E_1 of the backscattered particles. It is also evident from (2.2) that the energy of the particles scattered by the heaviest element is higher than those scattered by lighter ones. Furthermore, the energy E_1 of the projectile attains its maximum value for a scattering angle $\theta = 180°$. The importance of the kinematic factor is that it describes the reduction of incident energy during the collision, and this then allows identification of the mass of the target atom by measuring the scattered particles' energy.

2.2.2 Energy loss ($\frac{dE}{dx}$)

When an alpha particle penetrates a target it loses energy along its trajectory due to interaction with bound and free electrons in the target, and to small-angle nuclear collisions (with the later only being significant at low energies). The magnitude of the energy lost depends on the total distance travelled by the incident particle, and on the density and composition of the target,

University of Cape Town

as well as the incident particle's velocity (Feldman & Mayer 1986). The energy loss per unit length dE/dx at the energy E of the incident projectile is defined as

$$\lim_{\Delta x \to 0} \frac{\Delta E}{\Delta x} \equiv \frac{dE}{dx}(E), \tag{2.3}$$

for that particular particle and energy in that medium. When a projectile however undergoes a major collision with the target it can change its trajectory into an outward direction, but it will continue to lose energy until the alpha particles emerge. Figure 2.4 illustrated the energy loss for a projectile backscattered at a depth x. The energy of the incident particles is E_0, while the energy immediately before scattering at depth x is E. The energy after scattering is KE, while the energy of the particle emerging from the surface is E_1.

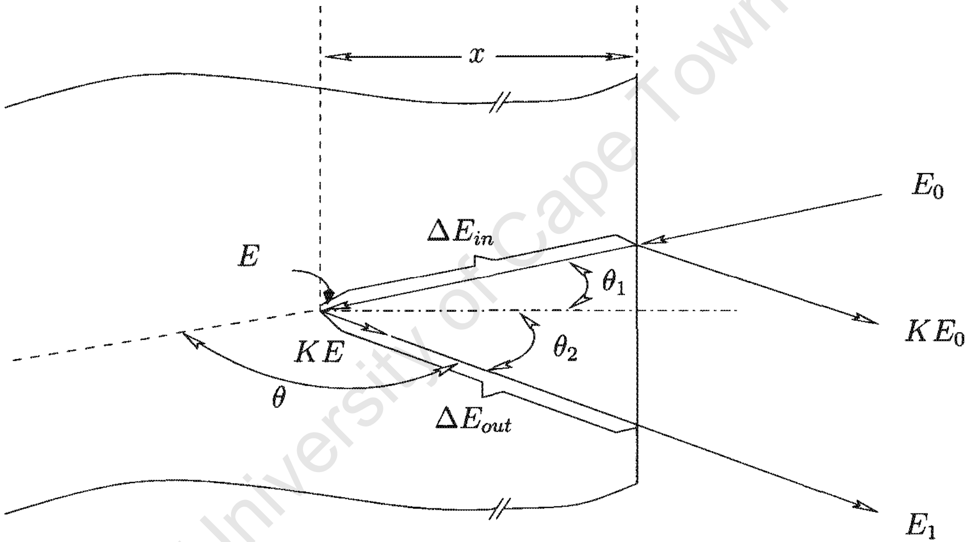

University of Cape Town

Figure 2.4: Illustration of the energy loss for a projectile backscattered at a depth x.

As shown in Figure 2.4 the energy loss can be described in three steps:

- Energy loss along the inward path ΔE_{in} (For an average energy loss on inward path of $\frac{dE}{dx}\mid_{in}$ resulting $\Delta E_{in} \cong \frac{x}{\cos\theta_1}\frac{dE}{dx}\mid_{in}$).
- Energy loss caused by the backscattering of the projectile ΔE ($\Delta E = E - KE$).
- Energy loss along the outward path ΔE_{out} (For an average energy loss on outward path of $\frac{dE}{dx}\mid_{out}$ resulting $\Delta E_{out} \cong \frac{x}{\cos\theta_2}\frac{dE}{dx}\mid_{out}$).

This is make it possible to determine the relation between the energy loss of the backscattered particles and the depth x

$$\Delta E \cong [S]x$$

where ΔE the energy difference between the particles scattered from the atoms at the surface and those scattered from atoms at depth x. The backscattering energy loss factor is given by:

$$[S] \cong \frac{K}{\cos\theta_1}\frac{dE}{dx}|_{in} + \frac{1}{\cos\theta_2}\frac{dE}{dx}|_{out} \tag{2.4}$$

By measuring the energy difference ΔE, the thickness of the sample can be determined from tabulated values of $\frac{dE}{dx}$ found in an earlier textbooks (Chu et al. (1978)). Today the thickness are determined by the simulation of the spectra using computer codes such as RUMP (Doolittle 1985), DataFrnace (Jeynes et al. 2003), SIMNRA (Mayer 2008), etc.

2.2.3 Differential scattering cross section ($\frac{d\sigma}{d\Omega}$)

The scattering cross section provides the relationship between the number of target atoms and detected particles. The number of particle that will be detected in a detector with solid angle Ω is given by

$$Y = \sigma(\theta)\Omega Q N_s \tag{2.5}$$

where $\sigma(\theta)$ is the scattering cross section i.e. the probability that a particle is backscattered towards a detector at an angle θ, N_s is the number of target atoms per cm^2 and Q the total number of incident particles (Chu et al. 1978, Feldman & Mayer 1986). By considering the Coulomb repulsion of two nuclei (which is the case in the RBS energy window), the differential scattering cross section can be determined (Chu et al. 1978) by the Rutherford scattering cross section in the laboratory frame of reference,

$$\frac{d\sigma}{d\Omega} = \left(\frac{Z_1 Z_2 e^2}{2E}\right)^2 \frac{\left[\cos\theta + (1 - M_1/M_2 \sin^2\theta)^{\frac{1}{2}}\right]^2}{\sin^4\theta(1 - M_1/M_2\sin^2\theta)^{\frac{1}{2}}}. \tag{2.6}$$

where Z_1 and Z_2 are the respective atomic number of the projectile of mass M_1 and target atoms of mass M_2. It is clear from equation (2.6) that the differential cross section $\sigma(\theta)$ depends on

University of Cape Town

Z_2^2, which indicates that RBS is significantly more sensitive to high Z elements. Therefore, if equal amounts of a light and heavy element are present, the number of particles scattered from the heavy element will be much greater.

2.2.4 Characteristics of an RBS spectrum

The RBS spectrum consists of a plot of the number of backscattered particles as a function of their energy. Figure 2.5 displays a measured backscattering spectrum for a CoSi, layer on Si. The bottom X-axis gives the channel number which is related to the backscattering energy in the top X-axis. The actual measured data is represented by squares and the simulation by RUMP is shown by the solid line.

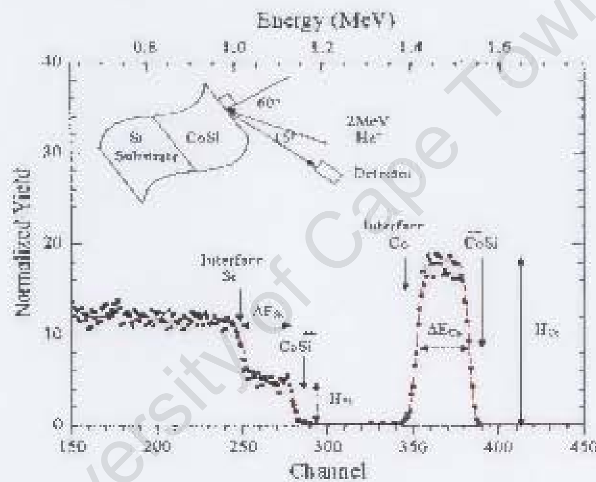

Figure 2.5: Rutherford backscattering spectrum of CoSi layer on Si.

University of Cape Town

In Figure 2.5 counts in channels 350-400 represent alpha particles scattered from Co atoms in CoSi film, while those between 250-285 represent scattering from Si in the CoSi film. Due to the larger kinematic factor, the signal that arises from alpha particles that scattered form the Co at the surface of the sample is found at channel 395 while that from Si is at channel 285. The rule is that the heavier the elements, the higher the energy of backscattered particles. Since cobalt is the heavier element, it shows energy peaks at higher channel numbers than those of the lighter element i.e. silicon.

The low energy edge of the Co spectrum around channel 350 arises of particles scattered from

the deepest part the CoSi film i.e. from near the interface between Si and CoSi layer. The energy loss by the alpha particles on the inward passage scattering and outward passages through the layer is indicated as ΔE on the spectrum, which corresponds to the energy difference between the edges. This is analogous to saying that atoms buried deeply in the sample will give a signal at a low channel number, while the same type of atoms near to the surface give a signal at a high channel number.

The step observed at channel number 285 is due to the scattering from silicon in the CoSi, while the sudden increase in backscattering yield at channel 240 indicates an increase in relative Si concentration at this depth. This therefore marks the interface between the silicide and the Si substrate. The width ΔE is related to the thickness of the film via the energy loss factor as given in equation (2.4). The depth at which the particle has penetrated can be determined by measuring the energy loss.

The height of the cobalt and the silicon signal represent the concentration of each element due to the differential cross section via equation (2.6) and is a measure for the composition of the phase that has been formed (one must note that RBS gives relative relation of the Co and the Si but not phase identifcation). The ratio of these heights is

$$\frac{H_{Co}}{H_{Si}} = \frac{\sigma_{Co}}{\sigma_{Si}} \cdot \frac{n_{Co}}{n_{Si}} \cdot \frac{[\epsilon_0]_{Si}^{CoSi}}{[\epsilon_0]_{Co}^{CoSi}} \tag{2.7}$$

where H_{Co}, H_{Si} are the signal height of the Co and the Si at the surface respectively, σ_{Co}, σ_{Si} are the cross section of the Co and the Si at the energy E_0 respectively, $\frac{n_{Co}}{n_{Si}}$ is the composition ratio, $[\epsilon_0]_{Si}^{CoSi}$ is the stopping cross section factor[1] for scattering from the Si in the CoSi layer, and $[\epsilon_0]_{Co}^{CoSi}$ is the stopping cross section factor for scattering from the Co in the CoSi layer (Chu et al. 1978). For the energy E_0 in the range 1-2 MeV, $[\epsilon_0]_{Si}^{CoSi} \cong [\epsilon_0]_{Co}^{CoSi}$ to within 10%, therefore the ratio of the stopping cross section term in equation (2.7) is $\cong 1$. Since in the CoSi layer $n_{co} = n_{Si}$, equation (2.7) can be approximated as

$$\frac{H_{Co}}{H_{Si}} \cong \frac{\sigma_{Co}}{\sigma_{Si}} \tag{2.8}$$

The difference in the heights of the Co and the Si observed in the spectrum is therefore essentially determined by the ratio of the scattering cross sections.

[1] See Chu et al. (1978) and Feldman & Mayer (1986) for definition

University of Cape Town

In this investigation the analysis of RBS spectra was performed using the computer software package RUMP (version 0.950) (Doolittle 1985). This program makes it possible to define a target that consists of a number of layers with different compositions and thicknesses. It simulates the resulting RBS spectra, based on the three aspects (discussed above) which underpin the rules of analysis of backscattering spectrum. The RUMP-code includes a very fast and powerful simulation package known as PERT that uses non-linear least square techniques to execute multivariable fits of simulated RBS spectra to experimental data. Once a qualitatively correct simulation is made, PERT varies selected parameters of the simulation to obtain quantitative results (Doolittle 1986). A recent paper by Barradas et al. (2007) has shown RUMP to be consistent and reliable, and that it compares favourably with other software such as DataFurnace (NDF) and SIMNRA for analysis of spectrum such as those obtained in this investigation.

University of Cape Town

2.2.5 *In situ* real-time RBS

The most convenient way to closely monitor the growth kinetics of the silicide in metal-silicon system is by ramped temperature annealing, as one can observe all the phases of the system from a single sample during one experimental run. In this investigation the onset and growth of cobalt silicides phase formation was monitored using *in situ* RBS while the sample undergoing a ramped thermal anneal. This technique is referred to as real-time RBS because the characterisation is carried simultaneously with the growth which occurs during the annealing. First recorded use of real-time RBS was to study the photodissolution of Ag in amorphous $GeSe_2$ (Rennie et al. 1986). The technique was improved and throughly investigated by Theron (1997). The advantage of real-time RBS over other *in situ* techniques such as XRD, and resistance measurements is that it provides a direct measurement of the thickness of the growing layer directly. For further information on real-time RBS readers consult Theron et al. (1998).

A rough sketch of *in situ* real-time RBS is shown in Figure 2.6. The sample was mounted on a cylindrical copper block used as a heating stage during *in situ* RBS measurement. To ensure good contact and thermal conductivity, a thin layer of conductive silver paste was used to stick the sample to the copper surface. The thermocouple was mounted from the back through a narrow hole in the copper block so that the tip was located inside the copper just below

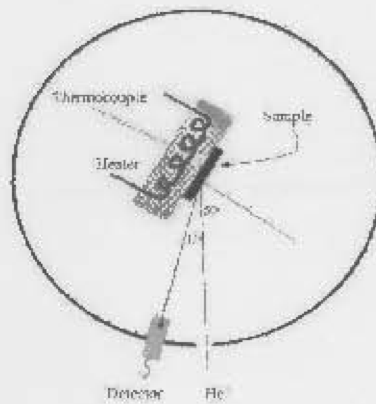

Figure 2.6: Real-time RBS setup.

the sample. The scattered particles have been detected with Ortec Ruggedized detector which has thin Al film cap layer to prevent photons emitted during the ramped thermal anneal from interfering with the measurements. To improve vacuum condition LN_2 reservoir was used which had added the advantage of keeping the detector cool during the ramp. In order to establish the true real-time temperature at the surface of the sample, the real-time system was calibrated by *in situ* resistivity measurement using a four-point probe. The thermal calibrations were made on Au/Si and Al/Si system at ramp rate of 2 °C/min (the same ramp rate was used during the measurements of the samples to avoid any problems caused by thermocouple time lag). These system have no intermetallic phases and a well defined eutectic (see the phase diagram of Au-Si in Figure 2.7), and a large and abrupt change in resistance therefore occurs at the eutectic temperatures.

University of Cape Town

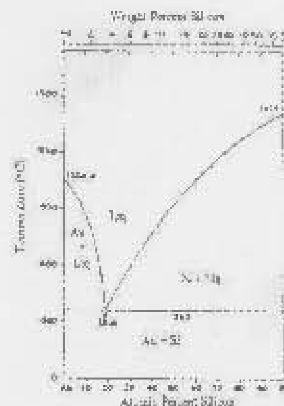

Figure 2.7: The phase diagram of Au-Si system figure reproduced from Okamoto & Massalski (1983).

Since the Au-Si eutectoid is 363 °C and that for Al-Si at 577 °C, these two points provide external references of the surface temperature of the sample in relation to that measured by the thermocouple. The relationship between measured temperature and surface sample temperature could then be determined by measuring the surface resistance of these two systems as functions of the thermocouple temperature. The temperature measured by thermocouple for the Au-Si eutectic was found at 369 °C, while that measured for Al-Si was 588 °C. The resistance versus temperature curve for the Au-Si system is presented in Figure 2.8.

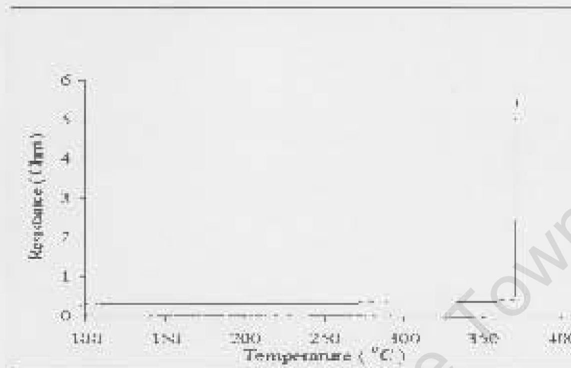

Figure 2.8: The resistance-temperature plot of Au-Si system showing an abrupt rise in resistance at 369 °C.

By assuming linear relationship between the two measured points, the temperature measured by the thermocouple was found to be given by $(0.977T + 2.42)$ °C with the result that the actual temperature was slightly lower than the measured temperature over the range of interest. (see Figure 2.9).

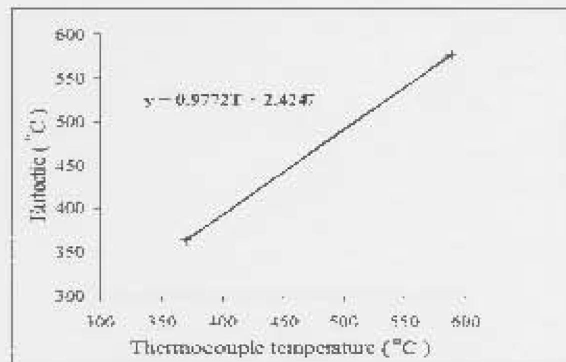

Figure 2.9: Thermocouple calibration made from the Au-Si and Al-Si systems.

For real-time RBS the samples were continuously analysed with 2 MeV alpha particles using an angle of incidence of 60 ° and a scattering angle of 165 °, while undergoing a ramped thermal anneal from 425 °C to 700 °C at a rate of 2 °C/min. To ensure a complete disilicide formation, some samples were then held at 700 °C for a further 30 minutes. Figure 2.10 shows the typical temperature profile during real-time RBS.

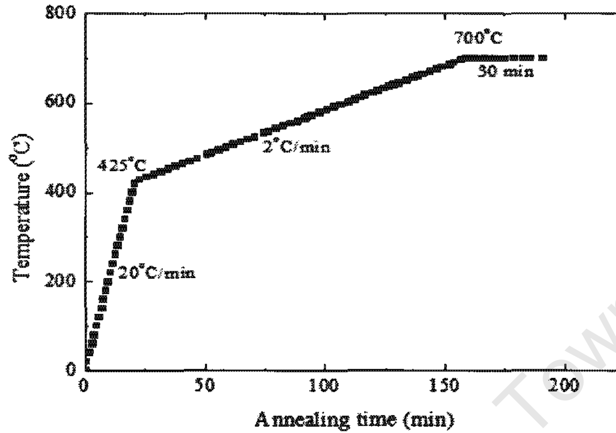

Figure 2.10: The temperature profile of a ramped anneal.

University of Cape Town

The thermal anneal was carried out at a pressure of about 2×10^{-7} torr. The beam spot size was 1 mm in diameter and the beam current was in the range 40 to 50 nA (Theron (1997) has shown that fluence of this order had little or no effect on the growth rate during silicide reaction). The temperature of the sample and the beam current was measured every 3s and RBS spectra were recorded every 30s. This resulted in the acquisition of over four hundred 30-s RBS spectra. In order to improve the statistics, four 30-s RBS spectra were added together. An example of the four spectra recorded over a 2 minute period around 536 °C is shown in Figure 2.11(a). The bottom part of the figure shows their composite RBS spectra. The scatter in the composite of two minutes spectra in Figure 2.11(b) is seen as acceptable and is easier to analyse as compared to the 30-s spectra in (a) where a large scatter in the data was observed.

Fluctuations in current were a common encounter during the analysis. Normalization of all the spectra in a given run was therefore required to correct this effect. This is easy to achieve by determining the integral number counts in an energy window where the spectrum remains constant throughout the reaction (e.g. Si in the substrate). The counts in each spectrum are then adjusted by a correction factor so that the integral over the energy window for that spectrum equaled the

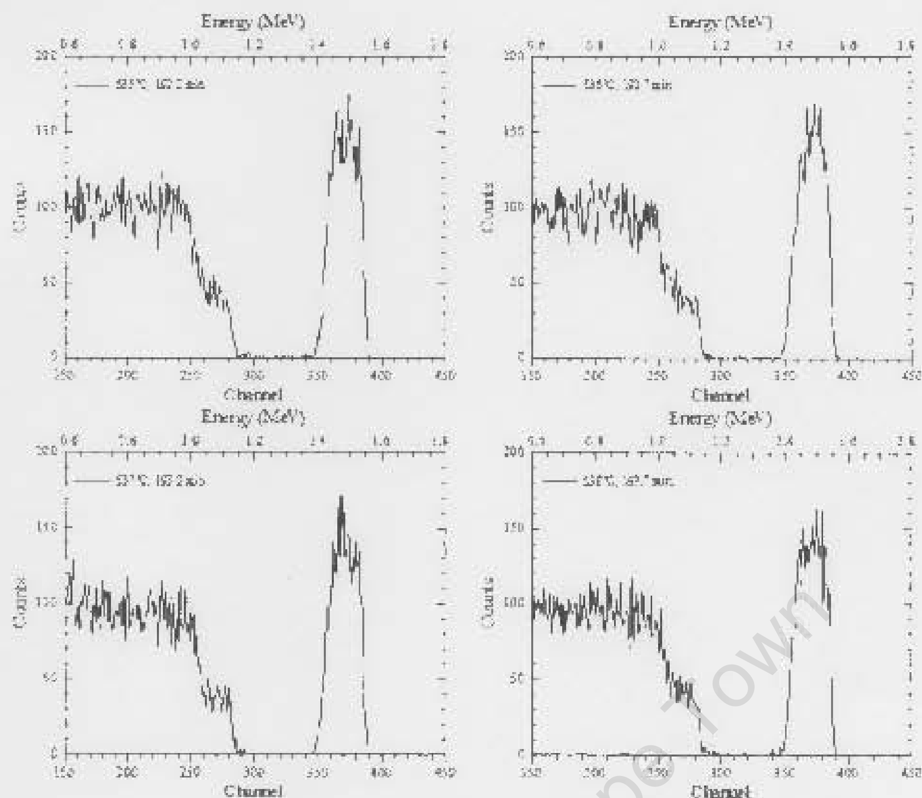

(a) Four 30-s RBS spectra.

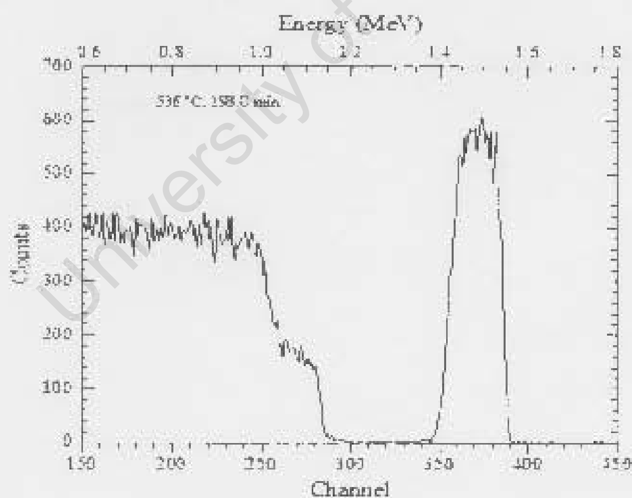

(b) Composite of 2-min spectra.

Figure 2.11: (a) Display of the four 30-s RBS spectra and (b) composite of 2-min spectra formed by merging the four 30-s spectra in (a) above.

University of Cape Town

average of all the spectra. Panel (a) in Figure 2.12 shows how the current was fluctuated during the analysis of Co deposited at room temperature. Panel (b) shows the 'effective' current after normalization.

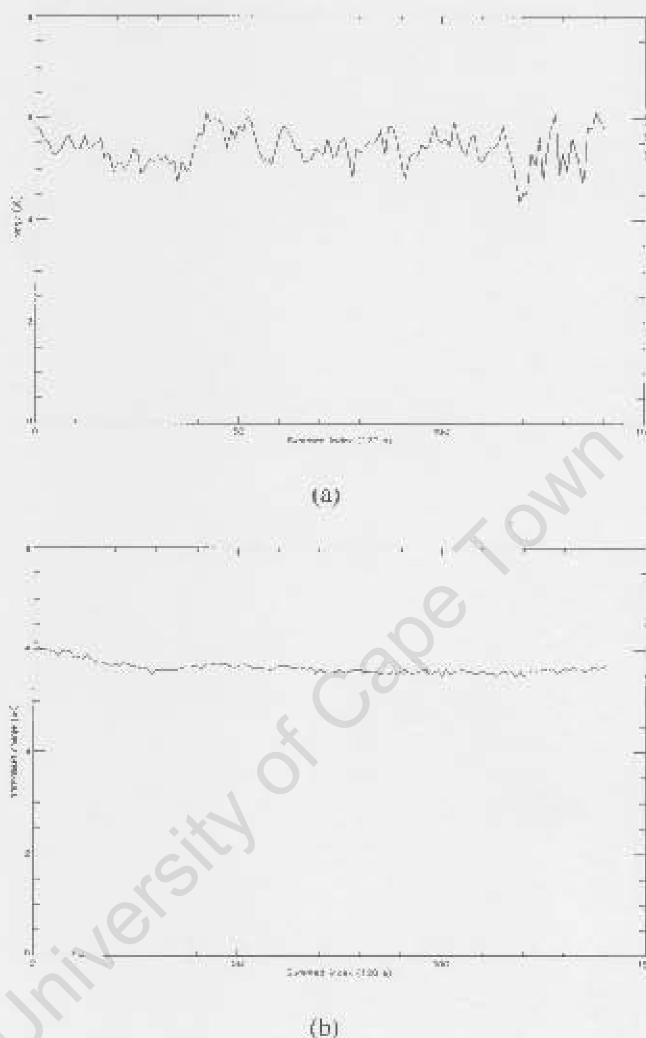

Figure 2.12: (a) The charge accumulation during the process of annealing. (b) the normalised charge showing the effective current after normalization.

2.3 X-Ray Diffraction

X-Ray Diffraction technique (XRD) is a widely used technique employed to study the crystalline structure of materials based on the ability of atoms to scatter X-rays. The principle of XRD is that a collimated beam of X-rays impinges on the sample and the intensity of the

University of Cape Town

diffracted beam is measured. This is observed only when certain geometrical conditions are satisfied, which may be expressed by the Bragg law.

$$2d_{khl} \sin \theta = n\lambda,$$

where λ is the incident X-ray beam wavelength, d_{khl} is the inter-planar distance for the hkl set of planes; θ is the angle to the diffraction plane and n is the order of diffraction. When these conditions are satisfied, a peak in the X-ray intensity will occur. A simplified geometrical picture of the scattering of an X-ray beam is illustrated in Figure 2.13.

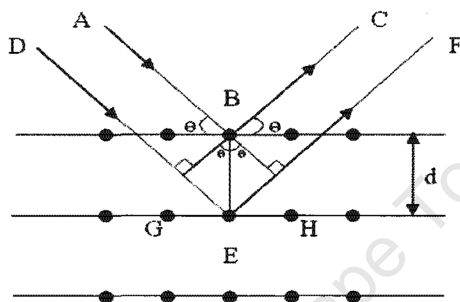

Figure 2.13: Reflection of X-rays from different atomic planes, illustrating Bragg's law.

University of Cape Town

As seen in Figure 2.13, the diffraction from a set of planes will only occur if the normal to these planes bisects the angle between the incident and the scattered beam.

In this investigation the real-time XRD measurements of the samples were performed at Gent University by J. Demeulemeester using a Bruker D8 diffractometer equipped with a custom built heating stage. It allows the identification of the phases (but provides no depth information) in a thin film because it determine the inter-planar distance d_{khl} (this inter-planar is characteristic for a silicide). The Cu K_{α} X-rays (wavelength of 1.54 Å) were used together with a linear detector [see Figure 2.14]. The incident angle θ was fixed at 24° and the detector was positioned at a fixed angle of 2θ = 51° but spaned a range of 2θ-values (Bragg condition will be fulfilled for planes that are parallel to the sample surface and for which the Bragg angle is equal to θ). The linear detector covered a window range between 41.5° and 60.5° (19°), allowing fast acquisition of the XRD spectra. The window range was chosen in order to incorporate intense

diffraction peaks of polycrystalline CoSi at 45.6 ° and 51.2 ° and $CoSi_2$ 47.9 °, together with a weaker $CoSi_2$ peak at 56.9 °. Ramped thermal anneals from room temperature to 900 °C were performed in an H_2 ambient at a linear heating rate of 1 °C/s. More detailed information on XRD technique can be found in Klug & Alexander (1974) and Sweet (2000).

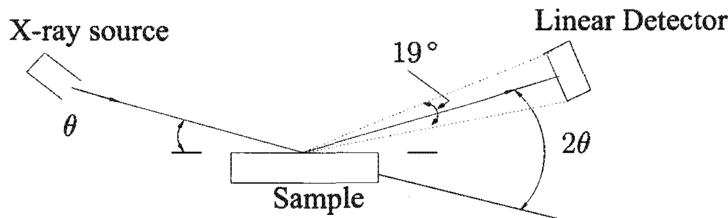

Figure 2.14: Schematic representation of the $\theta - 2\theta$ scan with a linear detector.

2.4 Atomic Force Microscopy

Atomic Force Microscopy (AFM) is a powerful tool to examine the roughness of surfaces (Magonov & Whqugbo 1996). Using an AFM, a sharp probe is scanned across the surface of a sample. The probe is a tip loaded on the end of a cantilever, which bends in response to the force between the tip and the sample. The cantilever is typically made of silicon or silicon nitride with a tip radius of curvature in the order of nanometers. The AFM operates using the principle of Hooke's law so that when the tip is brought into proximity to the sample surface, the force between the tip and the sample leads to a deflection of the cantilever. In contact-mode AFM the spatial variation of the tip-sample repulsive force, or that of the tip height, is converted into an image. The AFM can also be operated in the non-contact mode, where for instance the *van der Waals force*, the exchange force, or the magnetic force are detected.

A schematic of an AFM is shown in Figure 2.15 where the sample is mounted on top of a piezoelectric tube scanner that can move the sample in the z direction for maintaining a constant force, and the x and y directions for scanning the sample. The cantilever holder is fixed on top of the coarse and fine advance screws, with the tip positioned over the sample surface. The force between the sample and the tip is detected by the deflection sensor, and a topographic map of the sample surface can then be obtained by keeping the force constant while scanning the sample

University of Cape Town

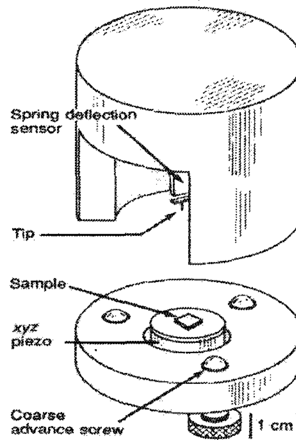

Figure 2.15: The atomic force microscopy (Chen & Waston 1999).

relative to the tip. Although there are several different techniques for detecting the cantilever deflections, a laser beam deflection system, introduced by Meyer and Amer in 1988 (Chen & Waston 1999) was used in this study. A schematic diagram of the optical beam deflection AFM is illustrated in Figure 2.16, where a laser beam is reflected by the top surface of the cantilever onto a position-sensitive detector. More detailed information on this technique can be found in Wiesendanger (1994). In this investigation the analysis of AFM images were performed using the computer software package Nanoscope v700.

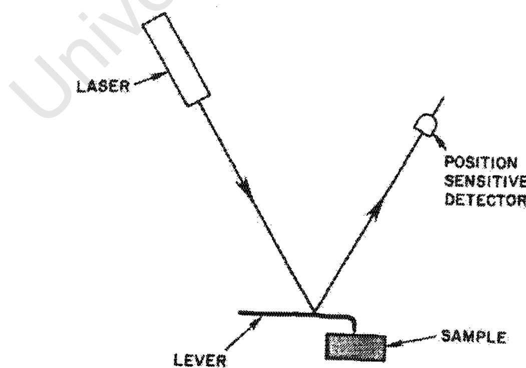

Figure 2.16: Detection of cantilever by optical beam deflection (Wiesendanger 1994).

University of Cape Town

Chapter 3

Results and Discussion

3.1 RBS analysis

3.1.1 Solid phase reaction results

The following are the results from Co deposited on Si<100> substrate at room temperature. During the analysis the sample was annealed over a temperature range of 200 – 650 °C at a rate of 2 °/min. The RBS spectra were obtained using 2 MeV alpha particles, and the analysis was performed using RUMP.

Figure 3.1 presents a three dimensional plot of the composite 2-minute RBS spectra obtained during the ramped thermal anneal. It presents a complete history of the reaction that occured in the sample, and thus provides a consistent picture of the interaction. However, it was difficult to extract qualitative information from it as some features are sometimes hidden behind others. It is therefore more productive to plot the data using contour lines as shown in the bottom part of Figure 3.1. In both panels the onset of the reaction between the Co film and the Si substrate to form Co_2Si is clearly visible, as is the onset of the formation of the $CoSi_2$ phase. However, it is difficult to tell when the CoSi began to form, and this information can only be obtained from a detailed analysis of the RBS spectra and is explained below.

The formation of the first phase, Co_2Si, was observed starting at a temperature of 365 °C as is shown in Figure 3.2. However, before the first phase completed its formation, the second phase,

University of Cape Town

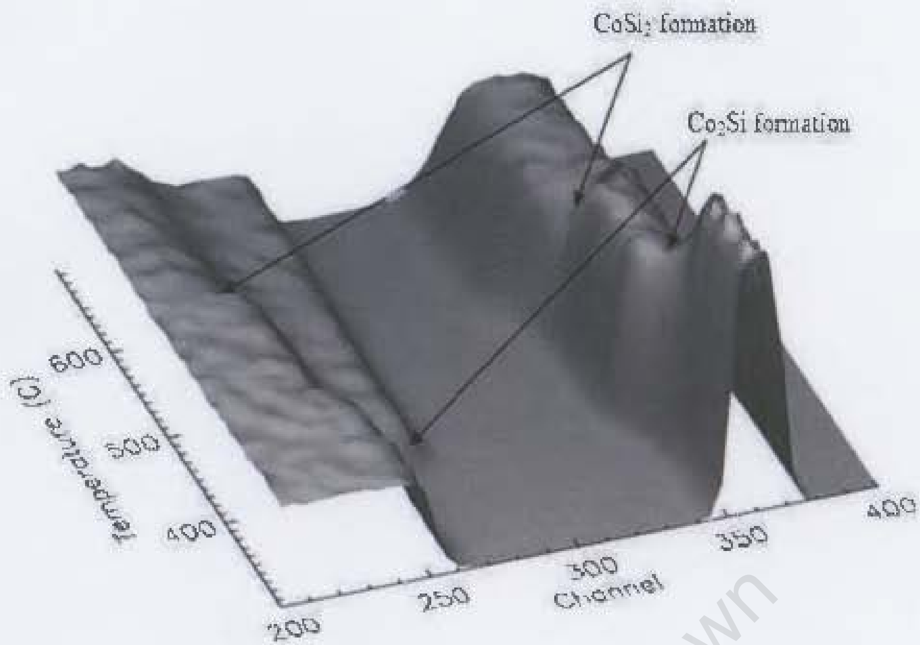

(a)

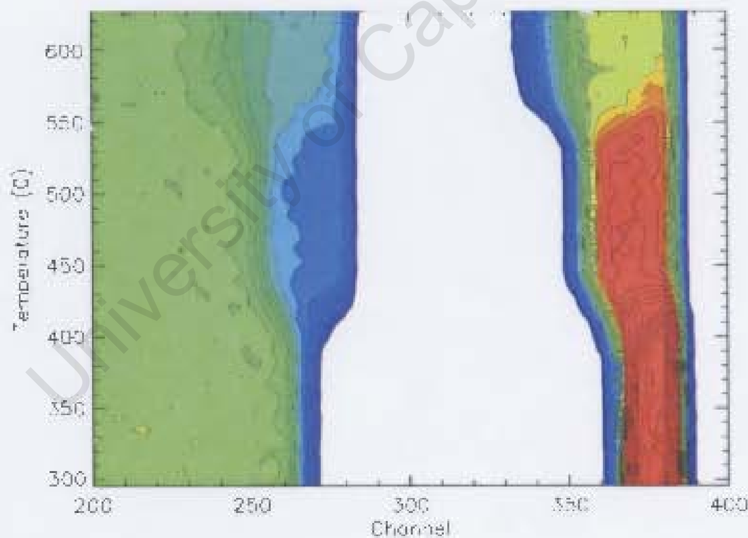

(b)

Figure 3.1: (a) Three dimensional plot of RBS spectra obtained during a ramped anneal (2 °C/min) of a 250 Å cobalt film deposited on silicon at room temperature. (b) Contour plot of the data in (a).

University of Cape Town

CoSi, began to grow at a temperature of around 405 °C, as shown in Figure 3.3. The cobalt was totally consumed at around 420 °C (i.e. no more surface cobalt was left to react with the

silicon). The first phase completed its conversion to the second phase at a temperature of around 440 °C, and Figure 3.4 shows that at 445 °C the film was entirely CoSi.

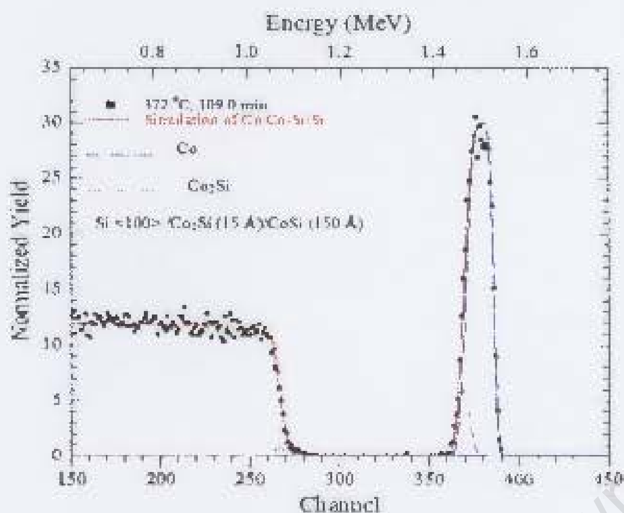

Figure 3.2: Backscattering spectrum showing Co_2Si growth at a thermocouple reading of 372 °C (calibrated temperature of 365 °C).

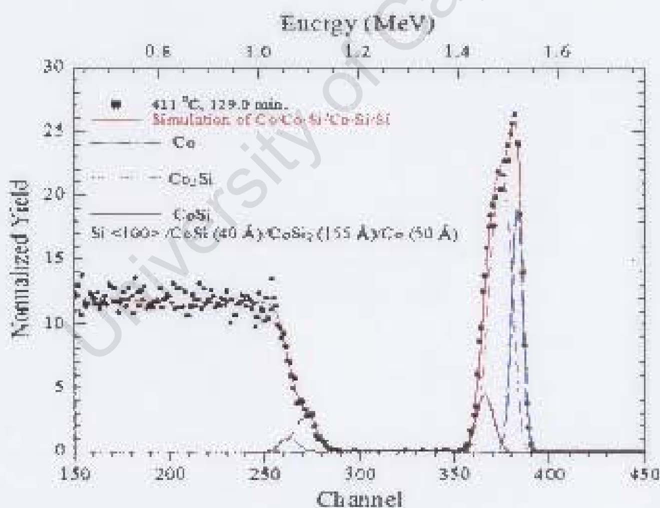

Figure 3.3: A backscattering spectrum shows CoSi begins to form at a thermocouple reading of 411 °C before all Co has been consumed (calibrated temperature is 405 °C).

The formation of the last phase, $CoSi_2$, was observed to begin at around 535 °C and the reaction completed (i.e all CoSi phase converted to $CoSi_2$ phase) at a temperature of around 600 °C. Figure 3.5 shows $CoSi_2$ phase when it started its formation around 535 °C and Figure 3.6 shows

University of Cape Town

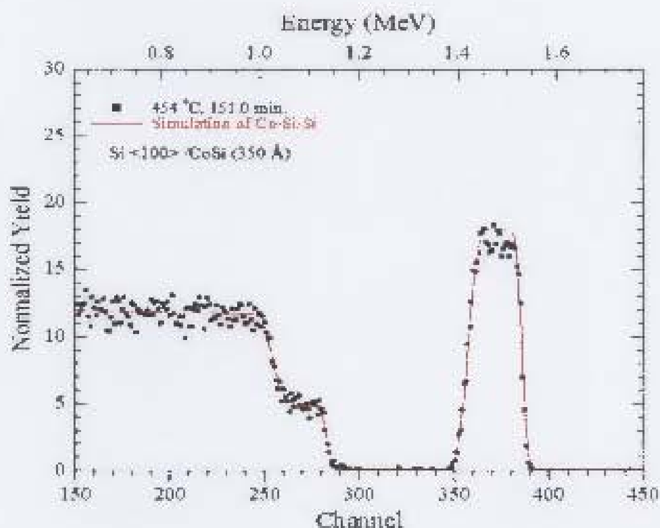

Figure 3.4: A backscattering spectrum showing complete growth of CoSi at a thermocouple reading of 454 °C (calibrated temperature is 445 °C).

a complete formation of $CoSi_2$ phase at a temperature of 605 °C.

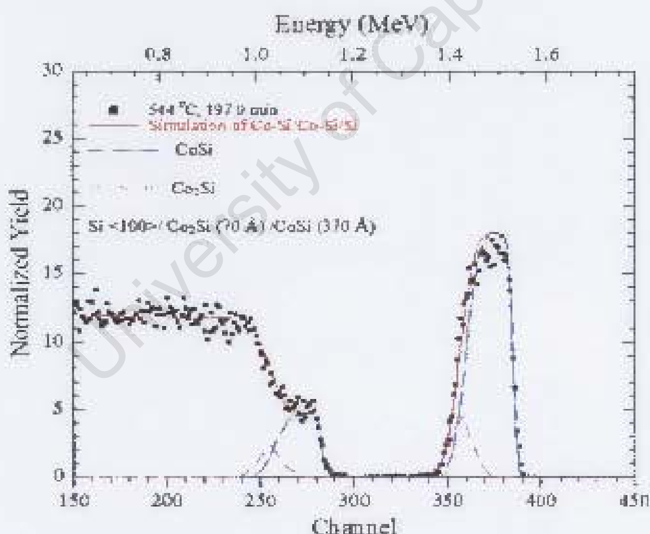

Figure 3.5: A backscattering spectrum showing the initial growth of $CoSi_2$ at a thermocouple reading of 544 °C (calibrated temperature is 535 °C).

The complete set of results obtained by simulation of real time spectra is displayed in Figure 3.7. The analysis confirmed that in Co/Si system, Co_2Si is the first phase, which begins to grow at a temperature of around365 °C, while the second phase, CoSi begins its formation at 405 °C.

University of Cape Town

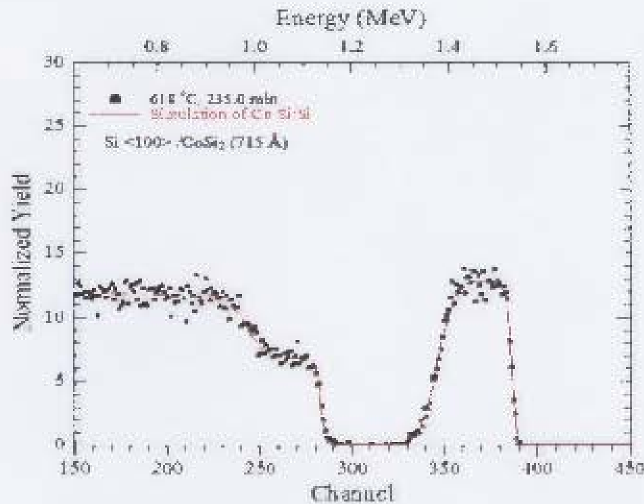

Figure 3.6: A backscattering spectrum showing a complete growth of $CoSi_2$ at a thermocouple reading of 618 °C (calibrated temperature is 605 °C).

The last phase, $CoSi_2$, started at a temperature of around 535 °C.

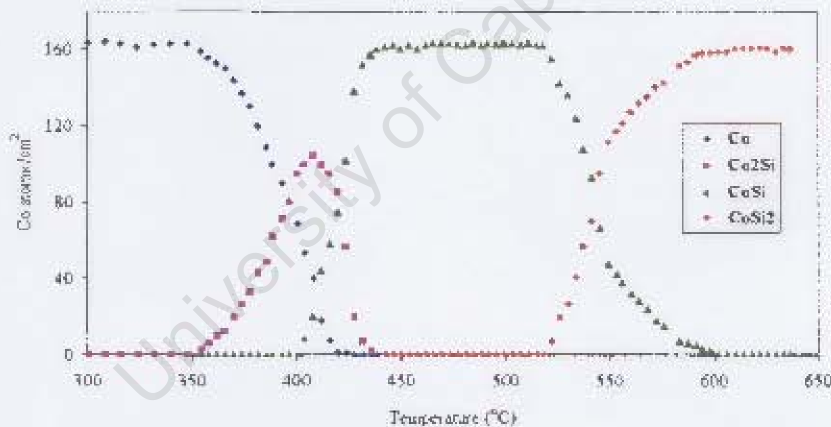

Figure 3.7: Results of the analysis obtained for Co deposited on Si at room temperature showing the formation of the various cobalt silicides phases.

In Figure 3.7 the number of Co atoms/cm^2 in each phase is plotted as a function of temperature. The plot was presented in this manner in order to cross check our analysis, since the total number of Co atoms in the film should remain constant throughout the reaction.

University of Cape Town

3.1.2 Reactive deposition results

As previously described, when cobalt evaporates under a UHV condition onto a heated silicon substrate, it reacts immediately with the silicon and forms cobalt silicides directly. Vantomme et al. (1996) demonstrated that if the substrate temperature is maintained above 550 °C a $CoSi_2$ film is produced, while when the substrate temperatures was lowered to 500 °C this resultled in an incomplete $CoSi_2$ reaction. This suggests that CoSi film can also be grown by means of reactive deposition. For the purposes of this investigation, films were grown at substrate temperatures ranging from 375 – 550 °C. Figure 3.8 shows XRD spectra for the set of as-deposited samples. The presence of CoSi peaks at $2\theta \sim 45.6°$ and $2\theta \sim 51.2°$ due to diffraction from the (210) and (211) planes of the CoSi phase respectively is clearly visible in all the samples.

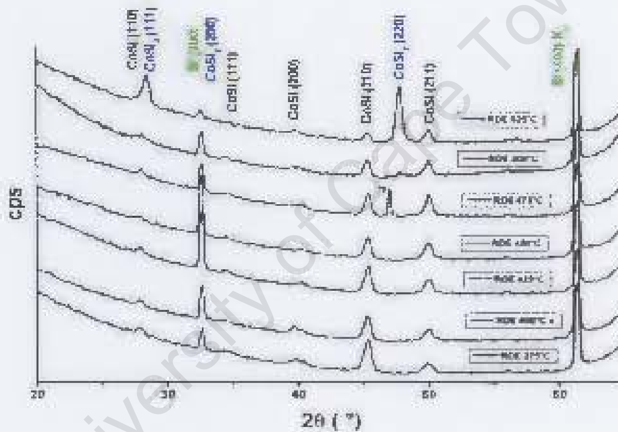

Figure 3.8: The XRD spectra for the set of samples (as-deposited) that were prepared by reactive deposition at temperatures ranging between 375 – 525 °C (measurements of XRD data performed by J. Demeulemeester at Gent University).

For the sample that was prepared by reactive deposition at 525 °C, an intense diffraction peak was also detected at $2\theta \sim 47.89°$ This is attributed to the (220) planes of the $CoSi_2$ lattice. The same diffraction peak was also found for the sample prepared at 500 °C although, it was less intensity compared to the sample prepared by reactive deposition at a temperature of 525 °C. As the magnitude of the spectral intensity is a rough measure of the quantity of the material present, it is possible to infer that a reactive deposition temperature of 500 °C has less amount

University of Cape Town

of $CoSi_2$ than that at 525 °C. A weak signal of $CoSi_2$ was also observed at $2\theta \sim 57.24°$ for CoSi film prepared at 500 °C and 525 °C reactive deposition temperatures.

It is believed that the peak observed at $2\theta \sim 47.2°$ for the sample that was prepared at 475 °C is not from the $CoSi_2$ phase as it too sharp to be a diffraction peak from a thin film. A weak signal was also been detected at around $2\theta \sim 28.2°$ due to the diffraction peak from the (110) planes of the CoSi phase. This shifts slightly to $2\theta \sim 29°$ for samples prepared at a reactive deposition temperatures of 500 °C and 525 °C which indicates the emergence of the the $CoSi_2$ phase.

The RBS spectra for the set as-deposited samples are shown in Figure 3.9. It can be seen from the figure that the spectrum of the sample prepared by reactive depositin at 500 °C is not significantly different to the spectrum obtained at 400 °C and 450 °C. This suggests that the film is largely in the form of CoSi and therefore that the amount of the $CoSi_2$ in the film is small.

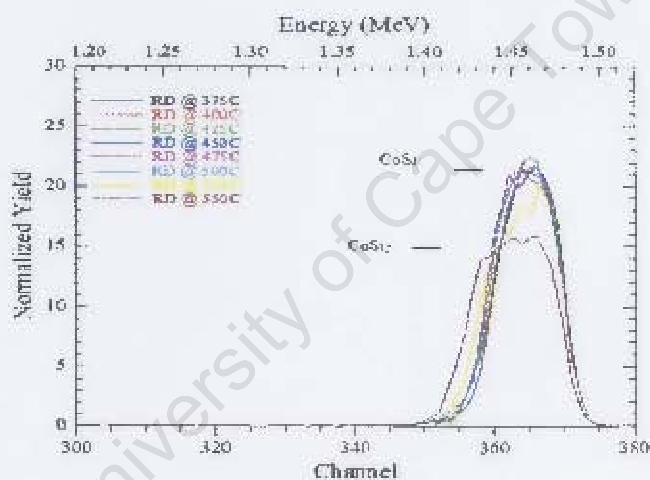

Figure 3.9: RBS spectra for the set of samples (as-deposited) that were prepared by reactive deposition at temperatures ranging between 375 – 550 °C (an angle of incidence of 10° was used).

As is shown in Section 3.1.1 the formation temperature of the $CoSi_2$ phase is well defined for CoSi grown by solid phase reactions. To investigate whether the reactive deposition temperature had any effect on the $CoSi_2$ formation temperature, all samples were analysised. Only the results from cobalt deposited at a reactive deposition temperature of 400 °C, 450 °C and 500 °C will be presented below in detail. The remaining samples are included in the appendices. Real-time RBS with a linear ramped anneal at a rate of 2 °C/min between 425 – 700 °C was used to study the formation of the $CoSi_2$ phase from the reactive deposited CoSi.

University of Cape Town

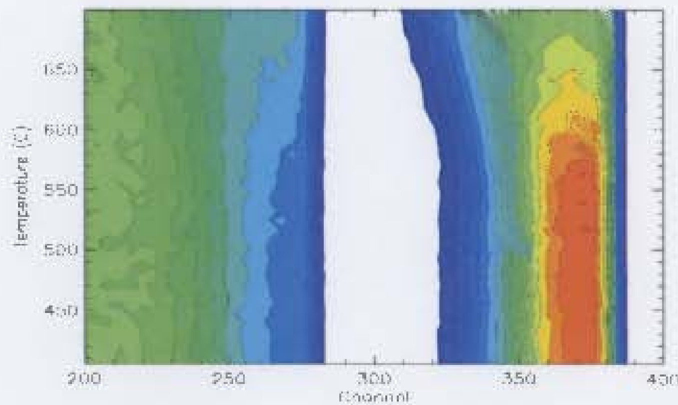

Figure 3.10: Contour plot of RBS data obtained during a ramped anneal (2 °C/min) of CoSi film prepared by reactive deposition at 400 °C.

Real-time RBS analysis of sample produced by reactive deposition at 400 °C:

Figure 3.10 shows a contour plot of the sample prepared at a reactive deposition temperature of 400 °C. The figure shows that the reaction starts at a temperature of around 580 °C. It can also seen that the reaction completes at a temperature of around 680 °C.

A spectrum such as that shown in Figure 3.11 was selected where it was clear that the film was in the form of CoSi. As is observed from the figure, the spectrum is broad and it has a tail on the low energy side of the Co peak. The XRD of the as-deposited sample showed that no $CoSi_2$ was present in the original sample. It is also evident from the contour plot in Figure 3.10 that no reaction had occurred by 270 °C. The CoSi tail is therefore clearly due to non-uniformity in the film, which makes it difficult to establish the onset temperature of $CoSi_2$. The spectrum was simulated by RUMP using a single layer of CoSi on Si substrate, and roughness (discussed later) of the film was measured to be about 6 nm.

A careful analysis of the spectra obtained during ramp annealing was undertaken using RUMP in the following manner. Roughness was taken into account using the Fuzz command in the RUMP program. The Fuzz was allowed to vary in PERT mode in order to obtain the best simulation . As the next higher temperature spectrum was simulated, the Fuzz value was monitored. When a sudden increase in the Fuzz was required by PERT to fit the spectrum, this was taken as an indication of the appearance of the $CoSi_2$ phase. The Fuzz value of CoSi layer in the

University of Cape Town

simulation was then fixed to the original value and the $CoSi_2$ layer was introduced.

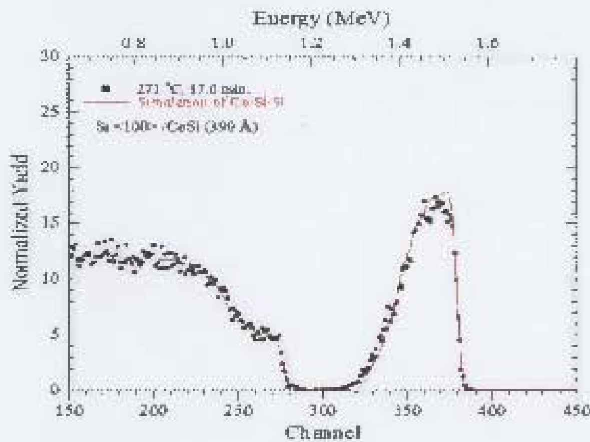

Figure 3.11: A backscattering spectrum showing CoSi film at a thermocouple reading of 271 °C (calibrated temperature of 267 °C) for the sample made by reactive deposition at 400 °C.

The analysis obtained for the sample showed that the formation temperature of $CoSi_2$ phase began at 575 °C, as displayed in Figure 3.12 together with its simulation. The CoSi phase was found to be completely converted to a $CoSi_2$ phase at a temperature of 670 °C as presented in Figure 3.13. The results of simulated real time spectra obtained for the entire ramp can be seen in Figure 3.14.

University of Cape Town

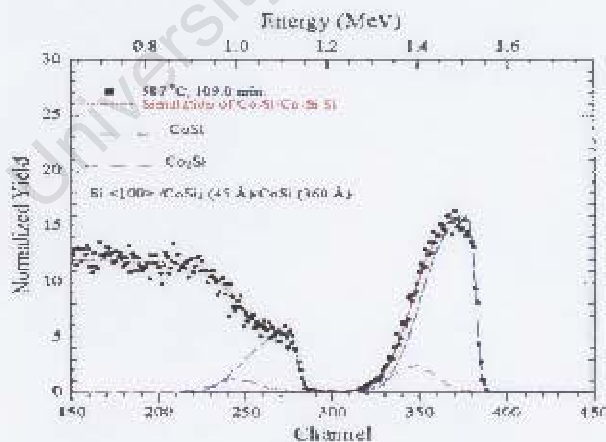

Figure 3.12: A backscattering spectrum showing the growth of $CoSi_2$ from CoSi by reactive deposition at 400 °C. The $CoSi_2$ starts its formation at a thermocouple reading of 587 °C (calibrated temperature of 575 °C).

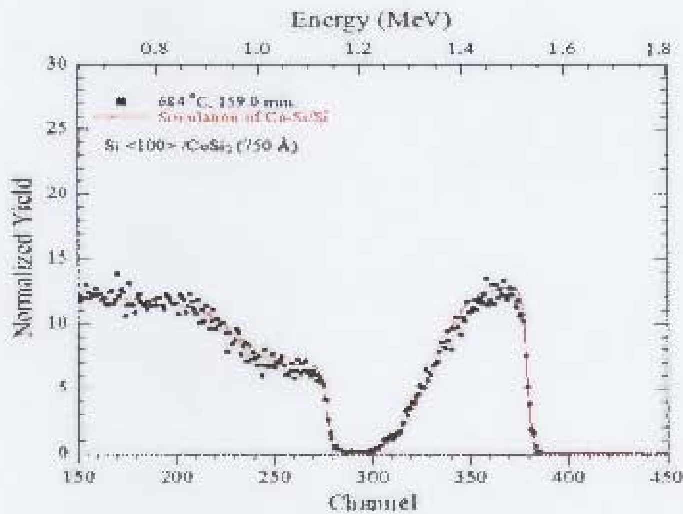

Figure 3.13: A backscattering spectrum of $CoSi_2$ grown from CoSi film produced by reactive deposition at 400 °C showing after all CoSi converted to $CoSi_2$ at a thermocouple reading of 684 °C (calibrated temperature of 670 °C).

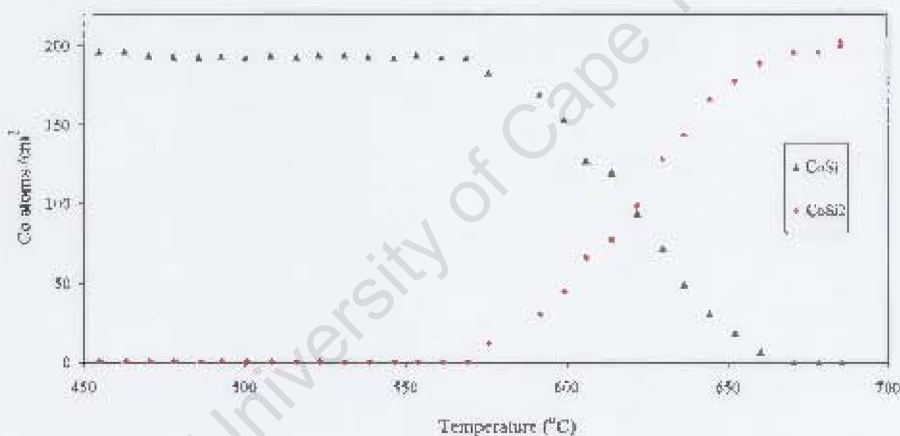

Figure 3.14: Results of the analysis of RBS spectra obtained from the sample produced by reactive deposition at 400 °C. The formation of $CoSi_2$ from CoSi initiated around temperature of 575 °C.

Real-time RBS analysis of a sample produced by reactive deposition at 450 °C:

Figure 3.15 shows a contour plot of the sample prepared by reactive deposition at a temperature of 450 °C. As can be seen from the figure the formation of $CoSi_2$ began at a temperature of around 500 °C and is separately displayed in Figure 3.16 with its simulation. A complete conversion of CoSi to $CoSi_2$ was found at a temperature of around 585 °C and is shown in

University of Cape Town

Figure 3.17. The complete set of the results from the simulated spectra obtained during the ramp are displayed in Figure 3.18.

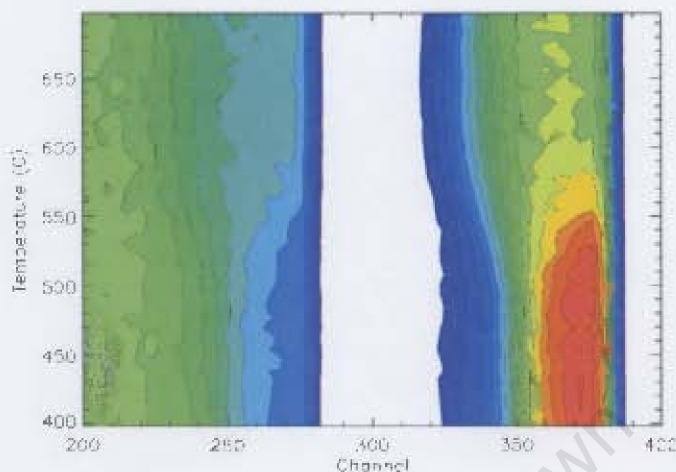

Figure 3.15: Contour plot of RBS data obtained during a ramped anneal (2 °C/min) of CoSi film prepared by reactive deposition at 450 °C.

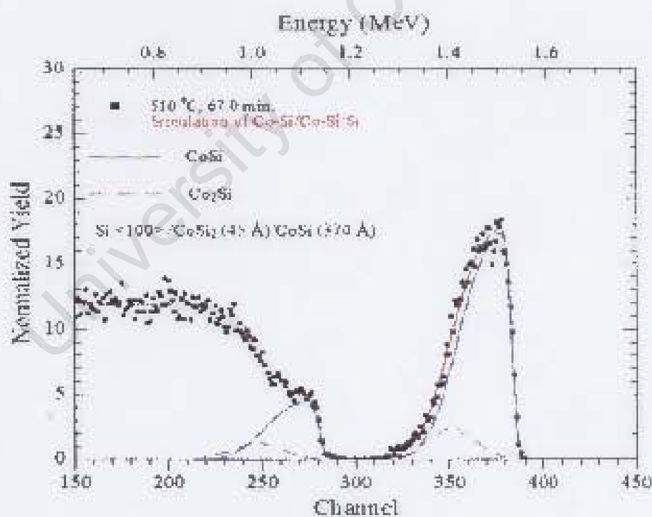

Figure 3.16: A backscattering spectrum showing the onset temperature of $CoSi_2$ at a thermocouple reading of 510 °C (calibrated reading of 500 °C) for the sample prepared by reactive deposition temperature at 450 °C.

University of Cape Town

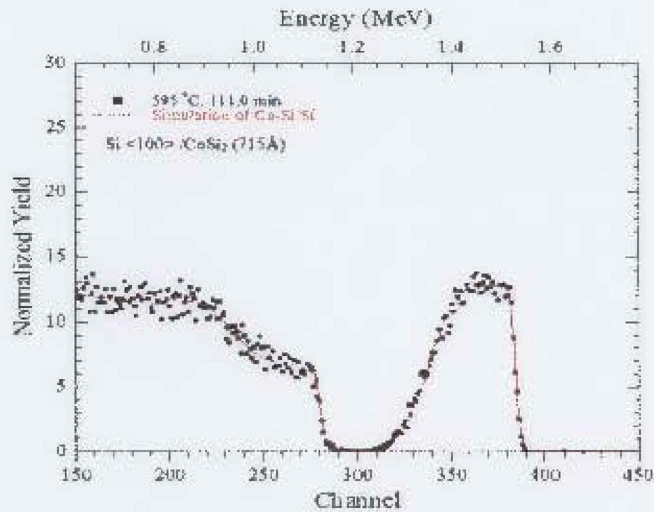

Figure 3.17: A backscattering spectrum showing when all CoSi phase converted to $CoSi_2$ phase at thermocouple reading of 595 °C (calibrated reading of 585 °C) for sample prepared by reactive deposition at 450 °C.

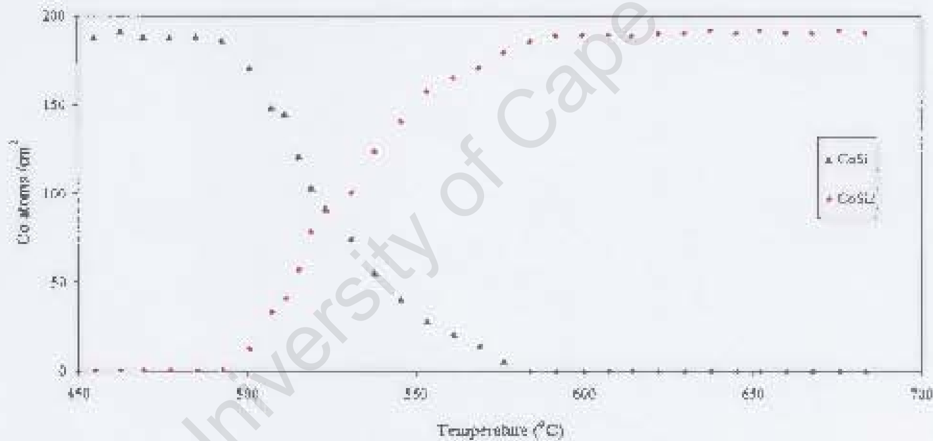

Figure 3.18: Results of the analysis of the RBS spectra obtained from the sample made at 450 °C reactive deposition temperature. The formation of $CoSi_2$ from CoSi began at a temperature of around 500 °C.

University of Cape Town

Real-time RBS analysis of sample produced by reactive deposition at 500 °C:

The formation of $CoSi_2$ was observed to begin at a temperature of 465 °C for the sample prepared at reactive deposition temperature of 500 °C (see contour plot in Figure 3.19). Figure 3.20 shows the onset of the $CoSi_2$ phase when it began to form at a temperature of 465 °C. The CoSi phase completed its conversion to $CoSi_2$ at a temperature of around 540 °C as presented in Figure 3.21. The complete set of the results from the simulated spectra obtained during the

ramp are displayed in Figure 3.22.

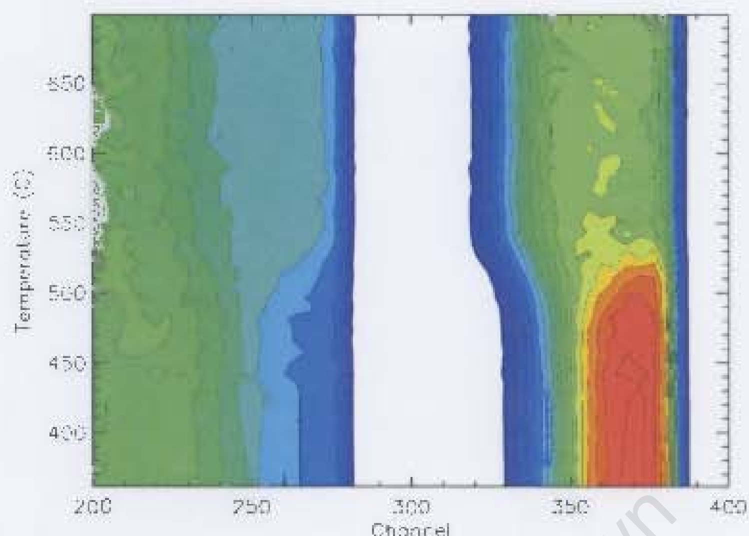

Figure 3.19: Contour plot of RBS data obtained during a ramped anneal (2 °C/min) of CoSi film prepared by reactive deposition at 500 °C.

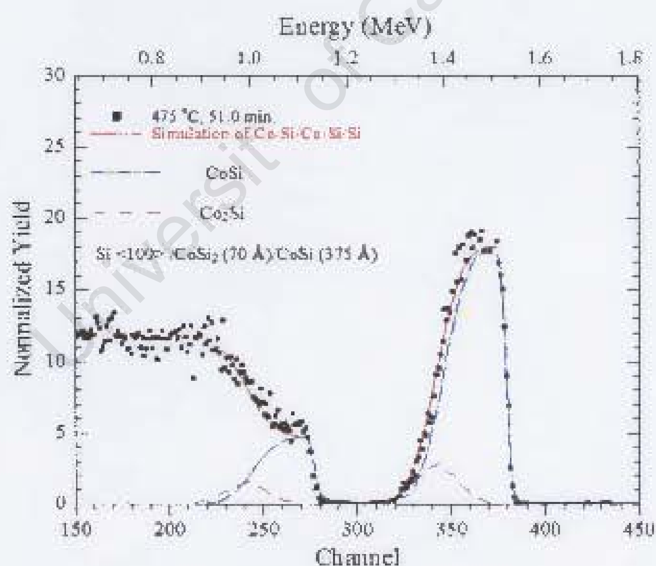

Figure 3.20: A backscattering spectrum showing the temperature at which $CoSi_2$ phase began its formation at a thermocouple reading of 476 °C (calibrated reading of 465 °C) for the sample prepared by reactive deposition at 500 °C.

In Figure 3.23 the onset formation temperatures of $CoSi_2$ from CoSi grown by reactive depo-

University of Cape Town

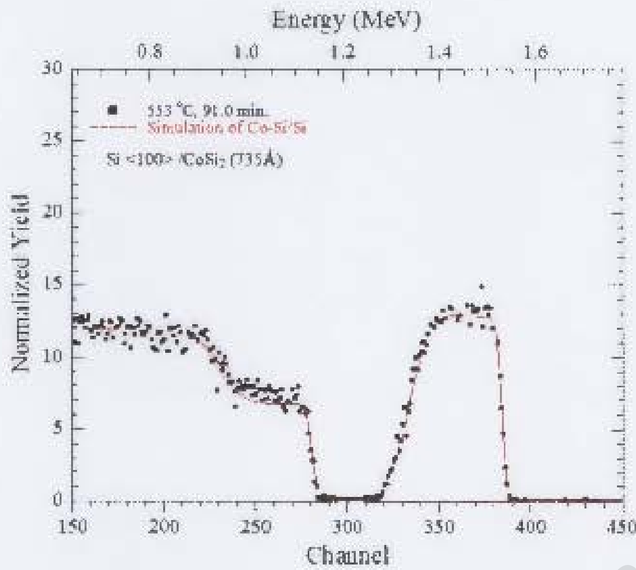

Figure 3.21: A backscattering spectrum showing when all CoSi phase converted to $CoSi_2$ phase at thermocouple reading of 553 °C (calibrated reading of 540 °C) for the sample prepared by reactive deposition at 500 °C.

University of Cape Town

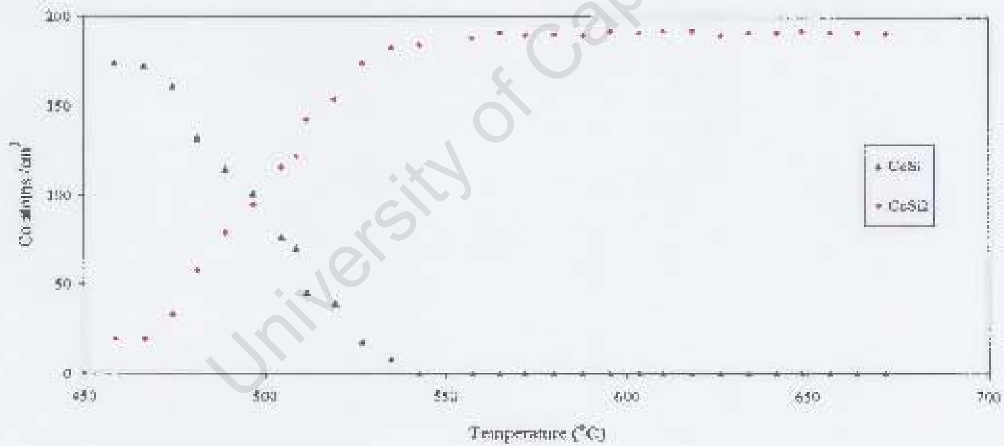

Figure 3.22: Results of the analysis of RBS spectra obtained from the sample prepared by reactive deposition at 500 °C. The formation of $CoSi_2$ from CoSi began at a temperature of around 465 °C.

sition at temperatures ranging from 375 – 525 °C were obtained by the simulation of real time spectra. The simulation results confirmed that $CoSi_2$ was present in the films grown by reactive deposition at a temperature of 500 °C and 525 °C (with ~ 6% being present in film grown at 500 °C and 20% being in film grown at 525 °C).

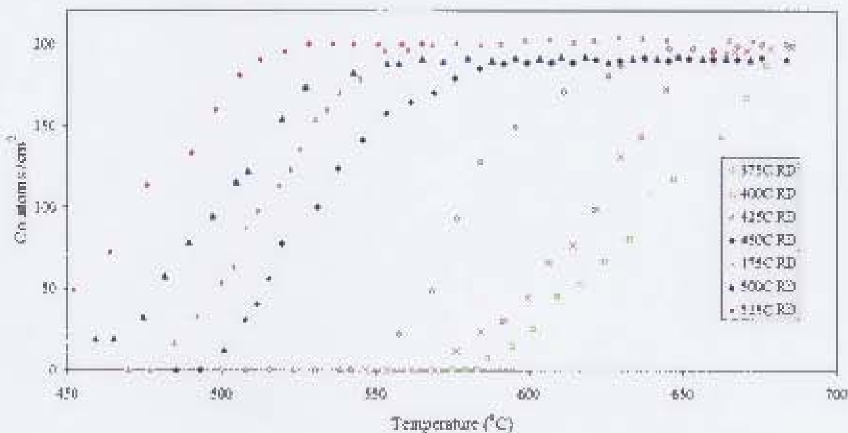

Figure 3.23: The onset formation temperatures of $CoSi_2$ produced from CoSi film prepared by reactive deposition at temperatures between 375 – 525 °C.

University of Cape Town

3.1.3 Co deposited at RT followed by a 450 °C anneal

As is evident from the above results, the formation of $CoSi_2$ from CoSi film grown by reactive deposition has different onset temperatures. To confirm that the onset temperature formation of $CoSi_2$ phase is not influenced by beginning the ramp with a sample in the CoSi phase, a portion of the Co/Si sample deposited at RT was annealed in a vacuum furnace for 30 minutes to convert it to CoSi. The CoSi film grown by solid phase reaction was then subjected to the identical real-time RBS analysis as undertaken by those CoSi films formed by reactive deposition.

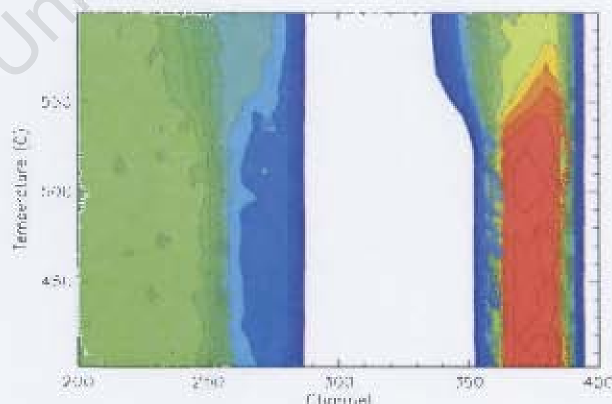

Figure 3.24: Contour plot of RBS data obtained during a ramped anneal (2 °C/min) of CoSi film prepared by solid phase reaction when the RT sample annealed to 450 °C.

Figure 3.24 shows a contour plot during the ramped anneal obtained for the sample. The growth of $CoSi_2$ phase is seen to begin at a temperature of around 535 °C as shown in Figure 3.25. A complete growth at a temperature of 575 °C for $CoSi_2$ is shown in Figure 3.26. The results from the simulation of the real time spectra are displayed in 3.27.

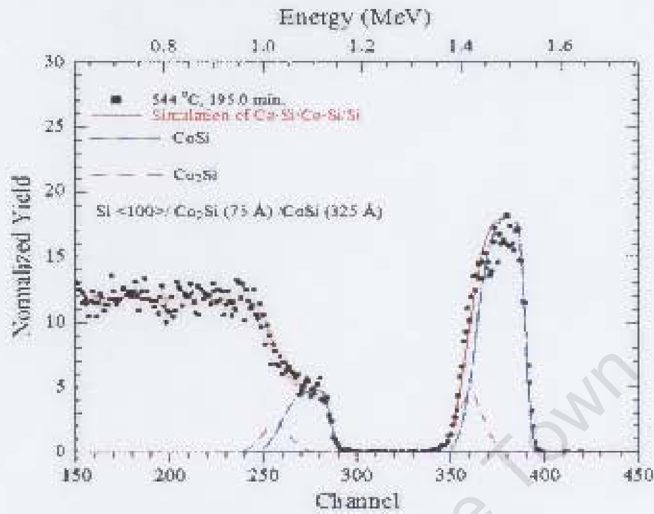

Figure 3.25: A backscattering spectrum showing when $CoSi_2$ is observed to begin its formation at a thermocouple reading of 544 °C (calibrated reading of 535 °C) for sample deposited at RT followed by 450 °C anneal.

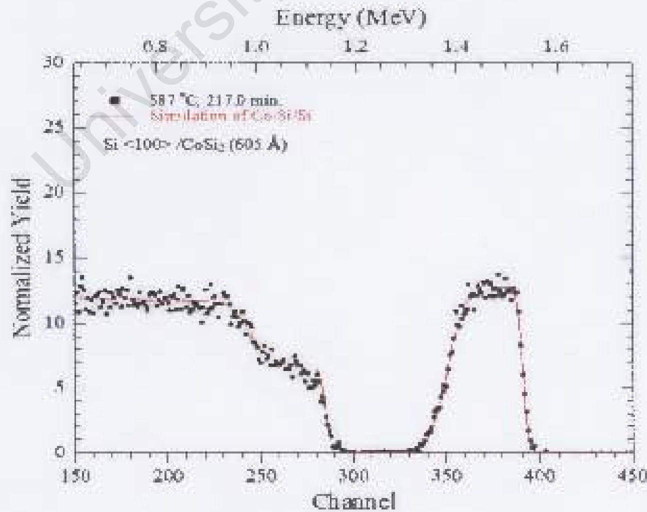

Figure 3.26: A backscattering spectrum showing a complete growth of $CoSi_2$ at a thermocouple reading of 587 °C (calibrated reading of 575 °C).

University of Cape Town

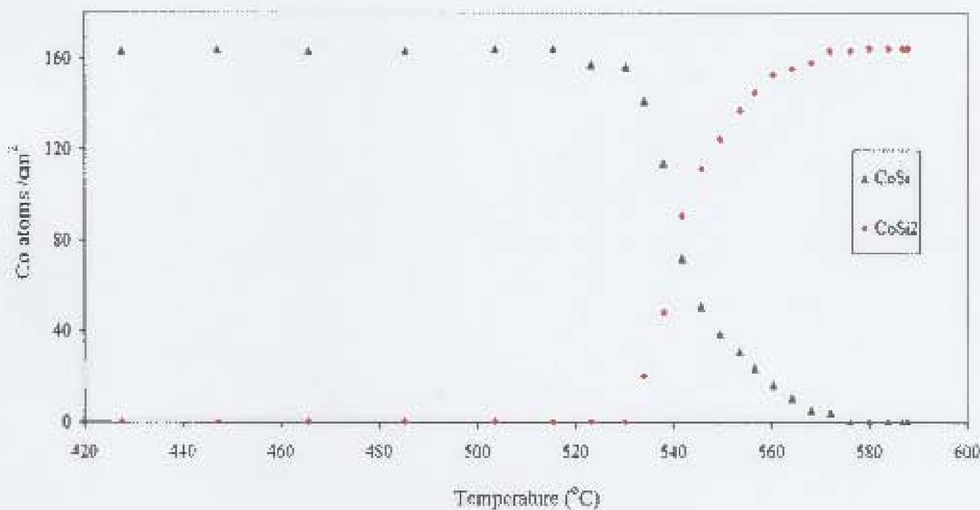

Figure 3.27: Results of the analysis of the RBS spectra for the sample deposited at RT followed by 450 °C anneal. The formation of $CoSi_2$ from CoSi initiated at a temperature of 535 °C.

3.2 Discussion

Co was deposited on Si at room temperature and then subjected to a linear ramp from 200 – 650 °C. Three distinct phases were observed to form at temperature ranges of between 360 – 605 °C. The precursor phase, Co_2Si, was observed between 360 °C and 435 °C. The second phase, CoSi was found to be present in the range between 405 – 600 °C. The last phase, $CoSi_2$ was observed to form at 535 °C. The same formation temperature was found when the sample was initially annealed at 450 °C to form CoSi phase. However, the temperature at which CoSi was prepared by reactive deposition was found to influence the formation temperature of $CoSi_2$. A significant difference in the onset temperature of the $CoSi_2$ phase was observed from around 575 °C from CoSi prepared by reactive deposition at 400 °C to about 465 °C for that prepared at 500 °C. For the sample prepared at a reactive depoistion temperature of 400 °C the CoSi phase was found to be entirely converted to $CoSi_2$ at a temperature of around 670 °C, while for sample preaperd at 500 °C all the CoSi was observed as converted to $CoSi_2$ at 550 °C. This indicates that the rate at which the CoSi phase is converted to $CoSi_2$ is faster when the sample is prepared at a higher reactive deposition. The full set of results from the real-time RBS investigation are plotted in Figure 3.28

University of Cape Town

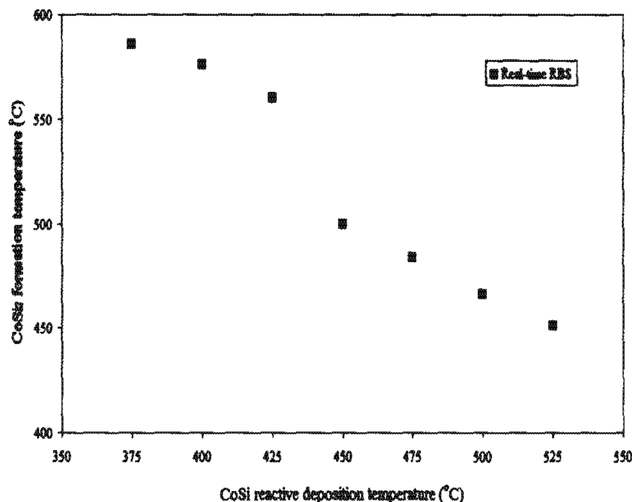

Figure 3.28: Temperature of onset of the formation of $CoSi_2$ from CoSi grown by reactive deposition at a temperature ranging from 375 °C to 525 °C.

3.3 XRD analysis

Identical samples prepared using a solid phase reaction technique were analysed using real-time XRD. The samples therefore underwent a ramped thermal anneal from room temperature to 900 °C at rate of 1 °C/s. Figure 3.29(a) shows real-time XRD contour spectra obtained during this procedure for the sample deposited at room temperature. Unfortunately reliable information could not be extracted about the silicides' formation from this technique due to the lack of a protective cap, which caused the Co film to oxidise rapidly during the ramp annealing. However, it was possible to perform real-time XRD on the CoSi film produced when the RT sample was subject to a 450 °C anneal to convert it to the CoSi phase, Figure 3.29 (b). The intense diffraction peaks at $2\theta \sim 45.6°$ and $2\theta \sim 51.2°$ [see Figure 3.29 (b)] indicate the presence of CoSi phase. The formation of $CoSi_2$ phase began at a temperature of around 560 °C, as is evident from the appearance of a diffraction peak of $2\theta \sim 48°$ in the figure.

All the CoSi films produced by reactive deposition were also subjected to real-time XRD analysis. The XRD spectra obtained during the ramped anneals from room temperature to 900 °C at rate of 1 °C/s of samples produced at reactive deposition temperatures of 400 °C, 450 °C and 500 °C are presented in Fig 3.30. From this figure, the diffraction peaks from CoSi are again clearly visible at $2\theta \sim 45.6°$ and $2\theta \sim 51.2°$, while the $CoSi_2$ diffraction peaks at $2\theta \sim 47.9°$

University of Cape Town

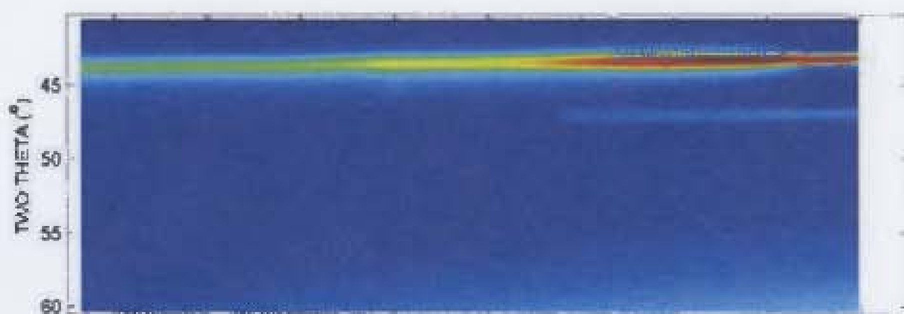

(a)

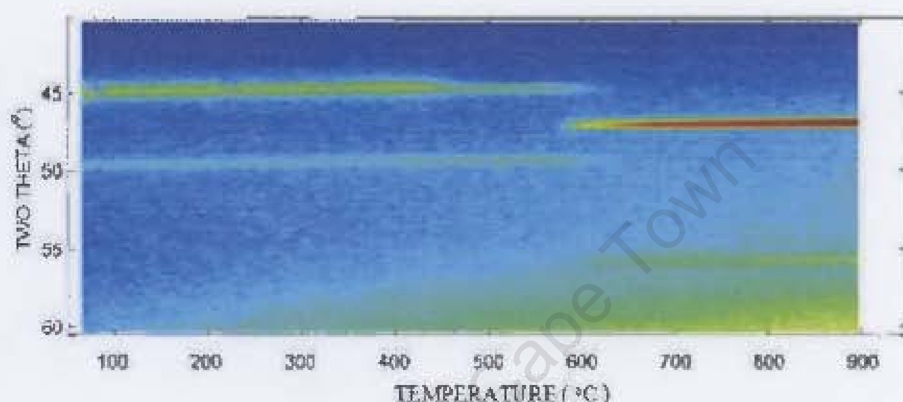

(b)

University of Cape Town

Figure 3.29: (a) The XRD data obtained during the ramp annealing at 1 °C/s of Co deposited at RT. (b) the XRD data for the same sample which had been pre-annealed at 450 °C to convert it to the CoSi phase. In both panels the formation of $CoSi_2$ phase was observed to appear at a temperature of 560 °C (measurements of XRD data performed by J. Demeulemeester at Gent University).

are also visible. The appearance of a less intense diffraction peak at $2\theta \sim 57.24°$ also indicates the formation of $CoSi_2$ phase. In Figure 3.30 (a), it can be seen that the onset temperature of $CoSi_2$ phase from CoSi prepared by reactive deposition at 400 °C was at a temperature around of 605 °C, and that the two CoSi peaks finally disappeared at 720 °C indicating that the reaction from CoSi to $CoSi_2$ was complete. As can be seen in Figure 3.30 panel (b) and (c) respectively, the formation temperature of $CoSi_2$ from CoSi reactive deposited at 450 °C was observed around 550 °C, and that reactive deposited at 500 °C was observed at 510 °C. The reaction for CoSi prepared by reactive deposition at 450 °C was completed by 630 °C while that for CoSi prepared at 500 °C was around 570 °C.

(a)

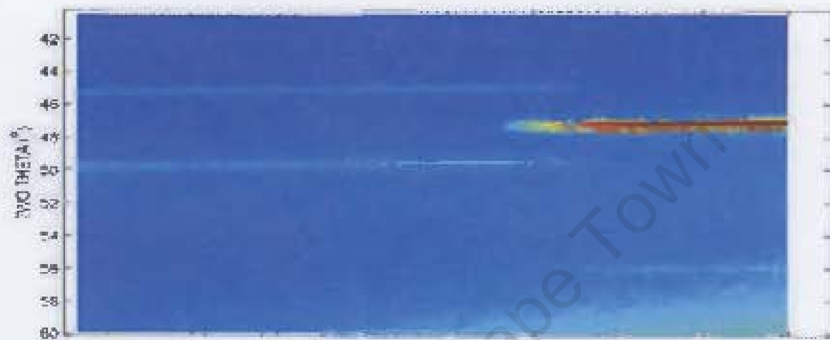

(b)

University of Cape Town

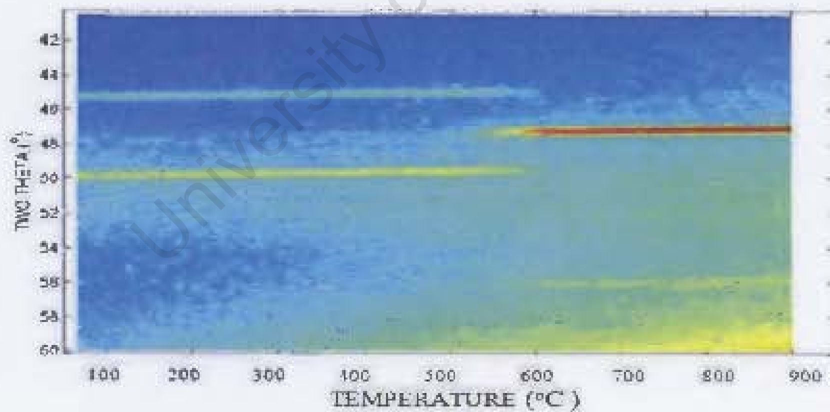

(c)

Figure 3.30: The XRD data obtained during the ramp annealing of Co reactive deposited at (a) 400 °C, (b) at 450 °C and (c) at 500 °C. The figure shows the formation of $CoSi_2$ phase, which begins at a lower temperature when the sample is prepared at a higher reactive deposition temperature (measurements of XRD data performed by J. Demeulemeester at Gent University).

3.4 Discussion

For samples prepared by solid phase reaction, it was only possible to obtain reliable information from Co deposited at RT and then annealed to 450 °C, as the CoSi film is less prone to oxidation than Co. The results showed that the formation of $CoSi_2$ from CoSi film produced by conventional solid phase reaction started at around 560 °C.

A different formation temperature of $CoSi_2$ was found when CoSi was produced directly by reactive deposition. For the CoSi film prepared at 400 °C reactive deposition temperature, the onset temperature of $CoSi_2$ was found at around 605 °C, while the CoSi phase was found to be entirely converted to $CoSi_2$ at a temperature of around 720 °C. For sample that was prepared by reactive deposition at 450 °C the $CoSi_2$ was found to begin its formation at 550 °C and all the CoSi was observed as converted to $CoSi_2$ at temperature of 630 °C . The formation of $CoSi_2$ by reactive deposition at 500 °C was found at lower temperature around 510 °C compared to that prepared at 400 °C and 450 °C reactive deposition temperatures. The CoSi film prepared by reactive deposition at 400 °C exhibits a slower rate of reaction when compared to the CoSi film prepared at 450 °C and 500 °C (the transformation from CoSi to $CoSi_2$ for 400 °C sample is completed over a temperature range of about 110 °C to 80 °C and 60 °C for that prepared 450 °C and 500 °C respectively). The full set of results for the real-time XRD investigation are plotted in Figure 3.31.

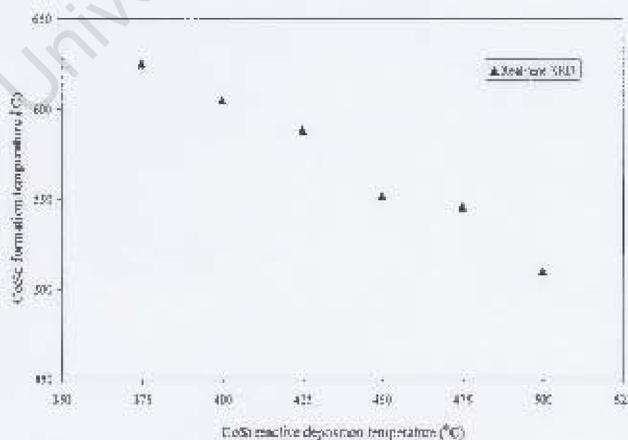

Figure 3.31: Temperature of onset of the formation of $CoSi_2$ from CoSi films grown by reactive deposition at temperature ranging from 375 °C to 500 °C.

University of Cape Town

3.5 AFM Analysis

Figure 3.32 shows three dimensional AFM images with a scan area of $5 \times 5\mu m$ of CoSi produced when Co has reactive deposited at $400\,^{\circ}C$, $450\,^{\circ}C$ and $500\,^{\circ}C$. From CoSi topographical image, the computer software package Nanoscope v700 calculated the average rms surface roughness of CoSi film prepared at a reactive deposition temperature of $400\,^{\circ}C$ [Figure 3.32 (a)] to be 6 nm. The average rms surface roughness measured for the CoSi film that was prepared at $450\,^{\circ}C$ [Figure 3.32 (b)] was found to be 4 nm and the same surface roughness was found for the sample that was prepared at a $500\,^{\circ}C$ [Figure 3.32 (c)].

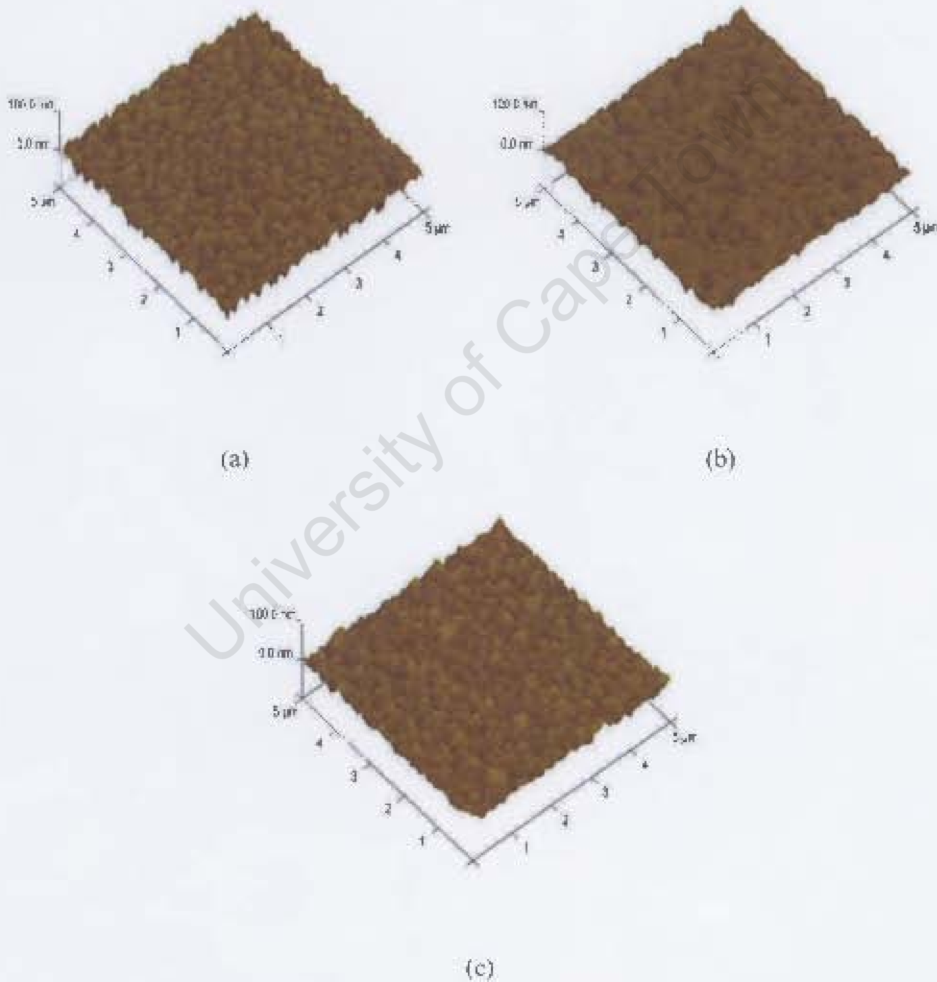

Figure 3.32: 3-D AFM images of CoSi film prepared by reactive deposition at (a) $400\,^{\circ}C$, (b) $450\,^{\circ}C$ and (c) $500\,^{\circ}C$.

University of Cape Town

In order to compare the roughness of the $CoSi_2$ film grown from the above CoSi films for the above samples, AFM measurements were also carried out on the $CoSi_2$ films formed by the ramped thermal anneal. Figure 3.33 shows the AFM images of $CoSi_2$ films obtained for the samples. From Figure 3.33 (a), the average rms surface roughness of $CoSi_2$ formed form CoSi film prepared at a reactive deposition temperature of 400 °C was measured to be 9 nm, while for $CoSi_2$ that was prepared at 450 °C was found to be 8 nm [see Figure 3.33 (b)] and that from CoSi film prepared at 500 °C [Figure 3.33 (c)] was determined to be 4 nm.

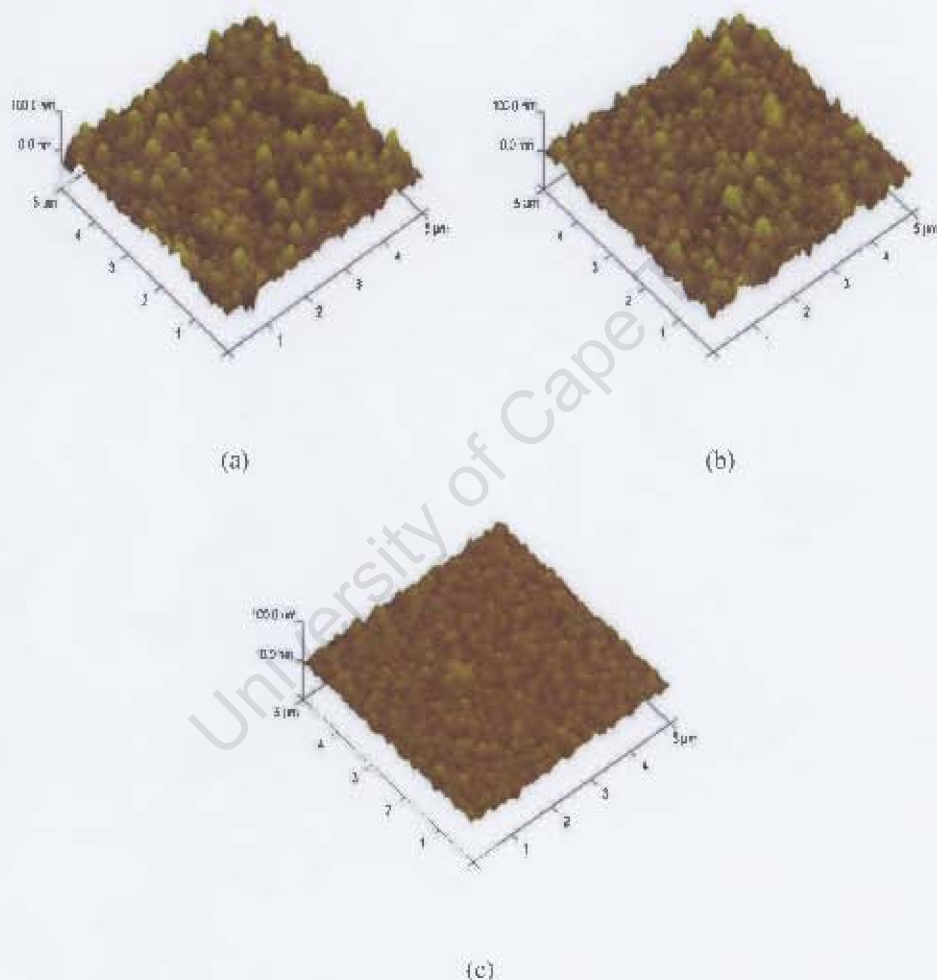

University of Cape Town

Figure 3.33: 3-D AFM images of $CoSi_2$ formed after ramped anneal of CoSi prepared at (a) 400 °C, (b) 450 °C and (c) 500 °C reactive deposition temperatures.

3.6 Discussion

The results revealed that all the surface films were found to be rough whether in the form of CoSi or $CoSi_2$. In the case of the former however, the CoSi film prepared at a reactive deposition temperature of 400 °C is rougher than that produced at 450 °C and 500 °C (i.e. about 6 nm for 400 °C compared with 4 nm for CoSi film prepared at 450 °C and 500 °C).

For the $CoSi_2$ film, there was apparently no big difference observed in the roughness of the sample prepared at a 400 °C and 450 °C reactive deposition temperature (the average rms surface roughness was calculated to be 9 nm and 8 nm respectively). A significant decreases in the roughness was however observed for $CoSi_2$ film grown from the sample prepared at a reactive deposition temperature of 500 °C where a roughness of about 4 nm was measured.

University of Cape Town

Chapter 4

Discussion

The investigation has shown that it is possible to grow CoSi film by reactive deposition. From the analysis of RBS/XRD of the films that were grown at temperatures ranging from 375 – 550 °C, it was found that for a substrate temperature maintained between 375 °C and 475 °C, the film is in the form of CoSi. Complete formation of $CoSi_2$ phase was observed for substrate temperature at $T = 550$ °C. When the substrate temperature was kept at $T = 500$ °C or 525 °C a mixture of mono/di-silicide was observed. However, the amount of the $CoSi_2$ that was found in CoSi prepared at a 500 °C reactive deposition temperature was small, while a significant presence of $CoSi_2$ was found in CoSi prepared at a reactive deposition temperature of 525 °C.

For silicides grown by solid phase reaction (cobalt deposited at RT and then subjected to linear ramp anneal from 200 – 650 °C), three distinct silicide phases were found in a temperature range between 360 – 600 °C. Detailed analysis of RBS data showed Co_2Si was the first phase to form and that is began to grow at about 365 °C. However, before Co_2Si completed its formation the second phase, CoSi, started to grow at a temperature of around 405 °C. The formation of $CoSi_2$, the last phase in cobalt silicide system, was observed as beginning at a temperature of 535 °C. The phase sequence and onset temperatures obtained from this investigation are in broad agreement with those in published literature (Gurp & Langereis 1975, Smeets 2007, Theron 1997).

The same onset temperature for a $CoSi_2$ phase was also found when the cobalt that was deposited at room temperature was annealed at a 450 °C to produce the CoSi phase. However,

University of Cape Town

the temperature at which CoSi was produced by reactive deposition was found to influence the subsequent formation temperature of the $CoSi_2$ phase.

For example, real-time RBS analysis showed that the formation of the $CoSi_2$ phase started at around 575 °C for CoSi film prepared by reactive deposition at a temperature of 400 °C, while it began at 465 °C for CoSi prepared by a reactive deposition at temperature of 500 °C. The RBS and XRD analysis of the remaining samples confirmed the same feature - the lower the reactive deposition temperature used to form the CoSi film, the higher the subsequent formation temperature of $CoSi_2$. A summary of the results obtained by RBS and XRD techniques is presented in Figure 4.1 which enables a comparison between the two techniques to be made.

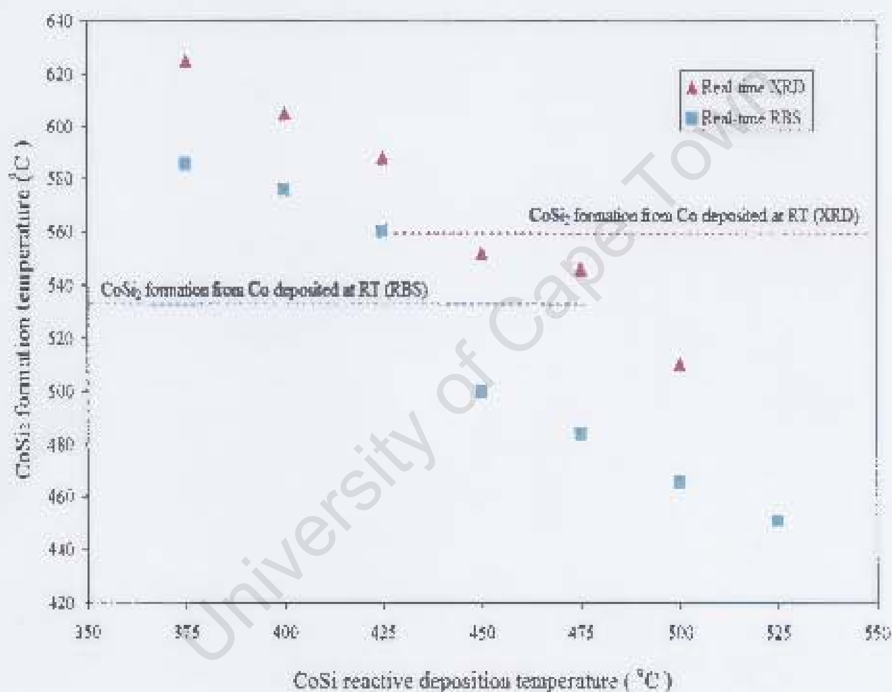

Figure 4.1: Graph displaying the onset temperature formation of $CoSi_2$ phase from CoSi-film prepared by reactive deposition at different temperatures (375 – 525 °C). The graph also shows the temperature formation of $CoSi_2$ prepared by solid phase reaction.

As can be seen from this figure, the real-time XRD results are in broad agreement with the real-time RBS data as the trend is essentially the same in both sets, while the average difference between the onset temperature measured by each technique can largely be ascribed to the higher heating rate used for the real-time XRD (1 °C/s for XRD compared to 2 °C/min for RBS).

The second major difference observed with the samples prepared by reactive deposition is the difference in their $CoSi_2$ rate of reaction. Although it was found that the reaction took place at lower temperatures for the samples prepared at higher reactive deposition temperatures, the rate at which the CoSi phase was converted to $CoSi_2$ was found to be faster. For instance, real-time XRD showed that it took a temperature range of 115 °C for CoSi film prepared by reactive deposition at 400 °C to fully convert to $CoSi_2$, while a temperature range of only 60 °C was necessary for CoSi reactive deposited at 500 °C. In other words, it took 115 seconds to convert CoSi to $CoSi_2$ for the sample prepared at a reactive deposition temperature of 400 °C, while it took 60 seconds to complete the reaction for the sample prepared at 500 °C. Furthermore, the longer reaction rate occurred at a higher temperature (i.e. 115 seconds at a temperature ranging from 605 – 720 °C compared to 60 seconds at a temperature 510 – 570 °C), contrary to what one expected as reaction normally proceed faster at higher temperatures.

The differences in the behaviour observed in this system is not obvious. A possible explanation for the lower nucleation temperature found in samples prepared at 500 °C and 525 °C (but not others) might be presence of $CoSi_2$ seeds in the CoSi films. However, the presence of such seeds would not explain the overall trend in the formation temperature of $CoSi_2$, as samples prepared at lower reactive deposition temperatures were found to nucleate at higher temperatures (seeds were only observed at reactive deposition temperatures of 500 °C and 525 °C). Another possibility for the lower nucleation could be due to different texture of CoSi films. It is also possible that stress could play a role in the onset formation temperature of $CoSi_2$ due to the immediate reaction between Co and Si.

University of Cape Town

The cause of the variation in the $CoSi_2$ growth rates could be due to the differences in microstructure, as it was observed that CoSi films grown at lower reactive deposition temperatures appeared to have larger grains compared to CoSi film grown at higher temperatures. This was clearly observed from the AFM images, and the same (i.e. larger grains) was also seen in the $CoSi_2$ film formed from the linear ramp. This is however unlikely to completely explain the variation in the $CoSi_2$ growth rate as the difference in the grain size (for example, the roughness that was found for CoSi film prepared by reactive deposition at 400 °C was 6 nm, while for CoSi film prepared at 500 °C it was to be 4 nm) for the CoSi films does not amount to much.

In the RBS contour plots of the CoSi film prepared at a reactive deposition temperature of

400 °C (Figure 3.10), the Co contours were observed to be more rounded at the high temperature ends, while they are more diagonal at 500 °C (Figure 3.19). This suggest that the growth of the $CoSi_2$ phase in the sample prepared by reactive deposition at 500 °C is more layer-by-layer, while the growth from that prepared at 400 °C is more columnar. The difference of the growth mechanism could therefore be another reason for the variation in the $CoSi_2$ growth rates.

It clearly what causes the difference in growth mechanism and the rate reaction for this system is is not yet fully understood but it is believed that the existence of seeds, texture and grain size and stress may have changed the number of nucleation sites which causes the differences in growth mechanisms. Further investigation into this system is thus clearly required. Cross-section Transmission Electron Microscope (TEM) measurement could identify the presence of $CoSi_2$ seeds as well as providing an indication of texture and grain size. The use of channeling technique could also assist to the texture analysis as well.

University of Cape Town

Chapter 5

Conclusions

In this work the formation of the $CoSi_2$ phase from CoSi films prepared by solid phase reaction, and by reactive deposition, have been investigated using real-time RBS and real-time XRD techniques. The surface roughness of the initial CoSi film and of the $CoSi_2$ formed during ramp, was also examined using the AFM technique.

By comparing the real-time RBS and XRD techniques which were used to study $CoSi_2$ formation, it is possible to conclude that either technique can be used to measure the onset temperature of $CoSi_2$ formation, but real-time XRD is faster (a measurement from room temperature to 900 °C is completed in around 15 minutes). It is also easier for detecting the onset formation of $CoSi_2$ (the emergence of the $CoSi_2$ phase is clear in XRD as the diffraction peaks are are well separated). The reaction rate can be obtained by both techniques, but only real-time RBS is able to provide quantitative data throughout the reaction period. Since RBS provides information regarding the composition as a function depth directly, it has the added advantage of being able to indicate where the reaction takes place.

In conclusion, the major findings from this investigation are:

1. The temperature of reactive deposition had a significant influence on the formation temperature of $CoSi_2$ phase, as it was found that the higher the reactive deposition temperature at which CoSi was produced, the lower the formation temperature of the $CoSi_2$ phase.

University of Cape Town

2. The temperature of reactive deposition also affected the rate of reaction, as it was observed that the higher the reactive deposition temperature the faster the reaction rate.

3. CoSi films grown at higher reactive deposition temperature had smaller grains. The $CoSi_2$ films grown during the ramped anneal showed similar behavior, with the films grown from CoSi produced at higher reactive deposition temperature having the smallest $CoSi_2$ grains.

4. The growth mechanism appeared to change in type from columnar growth for lower reactive deposition temperatures, to layer-by-layer for higher reactive deposition temperatures.

University of Cape Town

Appendix A

The formation of $CoSi_2$ from CoSi film prepared by reactive deposition at 375 °C

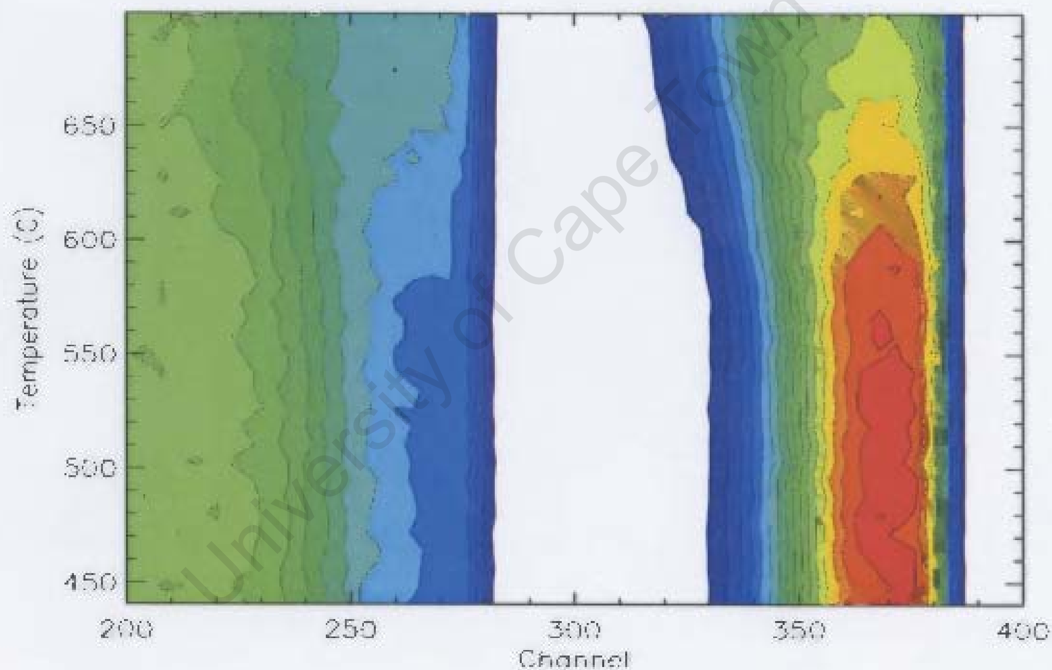

University of Cape Town

Figure A1: Contour plot of RBS data obtained during a ramped anneal (2 °C/min) of CoSi film prepared by reactive deposition at 375 °C.

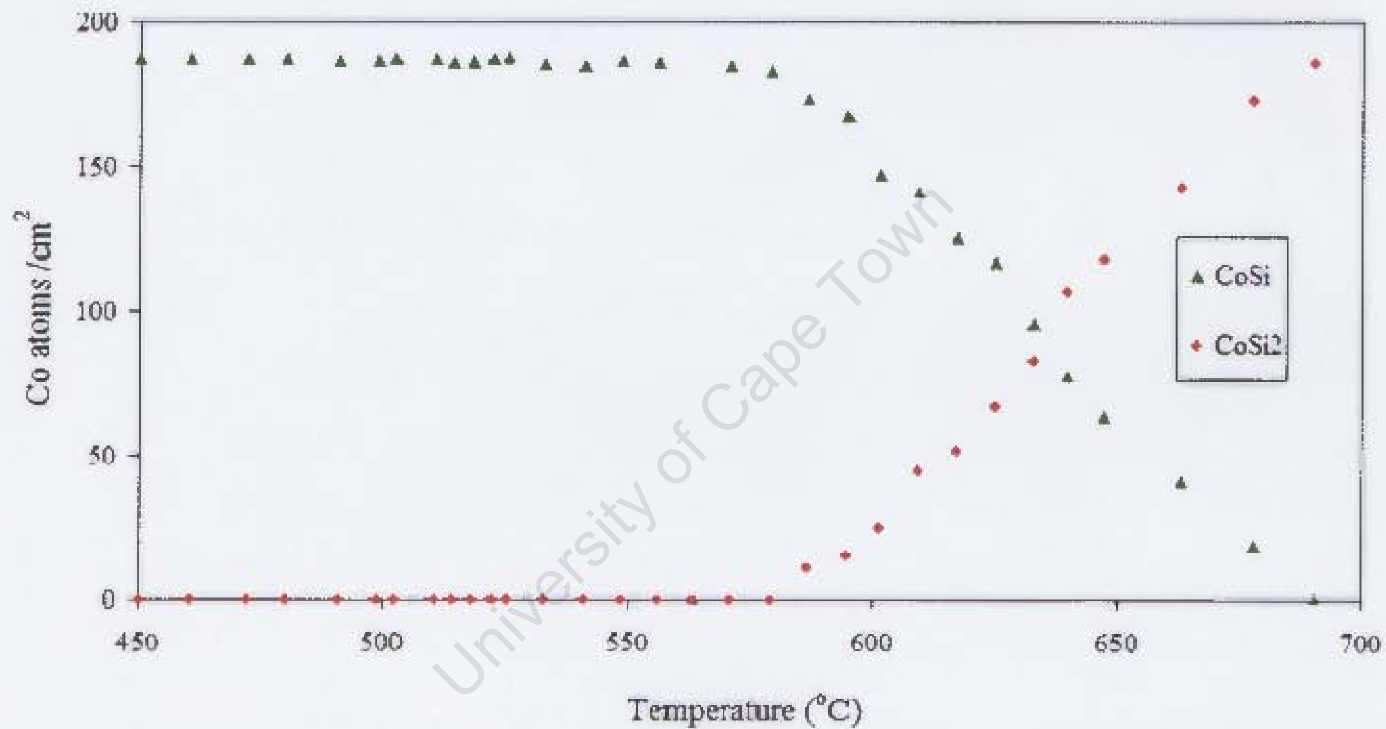

University of Cape Town

Figure A2: Results of the analysis of RBS spectra obtained form CoSi prepared by reactive deposition at 375 °C. The formation of $CoSi_2$ from CoSi initiated at calibrated temperature of 585 °C.

The formation of $CoSi_2$ from CoSi film prepared by reactive deposition at 425 °C

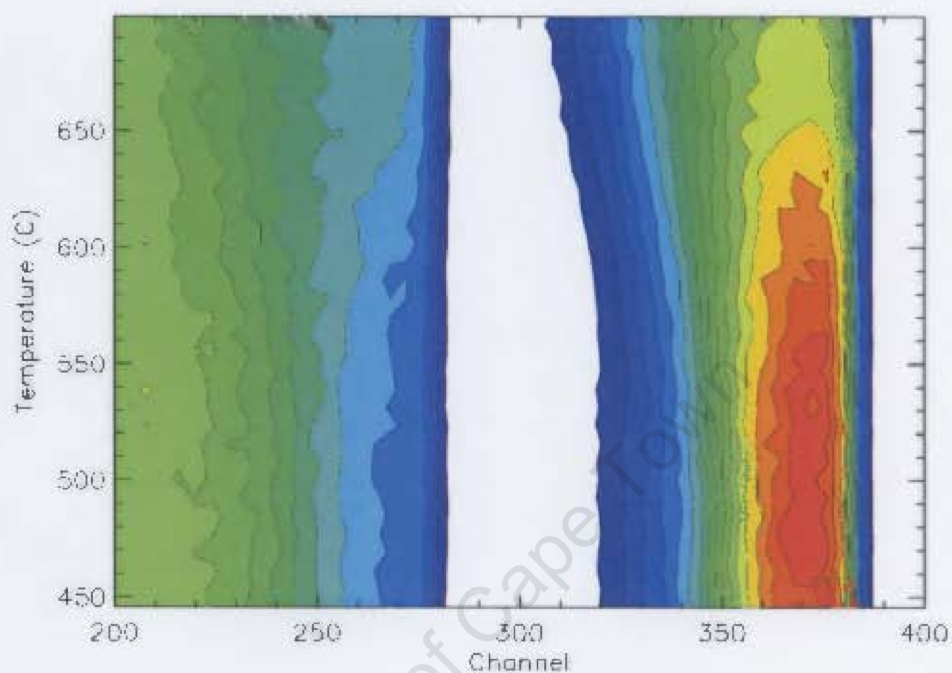

Figure A3: Contour plot of RBS data obtained during a ramped anneal (2 °C/min) of CoSi film prepared by reactive deposition at 455 °C.

University of Cape Town

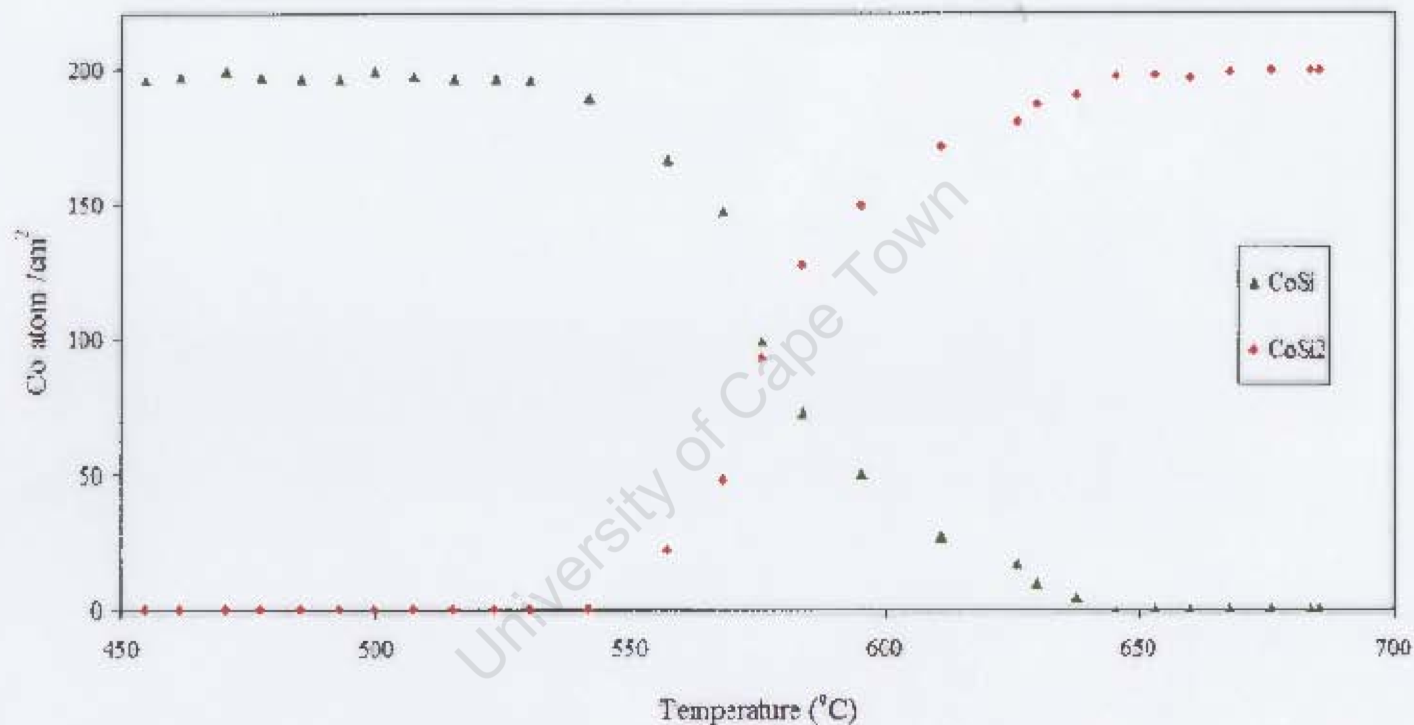

University of Cape Town

Figure A4: Results of the analysis of RBS spectra obtained form CoSi prepared by reactive deposition at 425 °C. The formation of $CoSi_2$ from CoSi started at calibrated temperature of 560 °C.

The formation of $CoSi_2$ from CoSi film prepared by reactive deposition at 475 °C

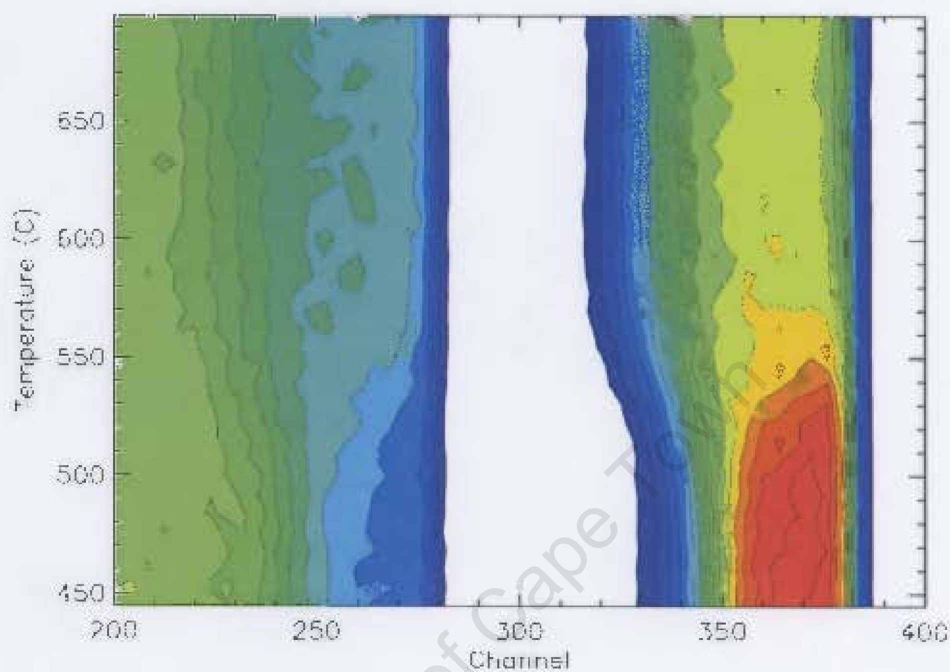

Figure A5: Contour plot of RBS data obtained during a ramped anneal (2 °C/min) of CoSi film prepared by reactive deposition at 475 °C.

University of Cape Town

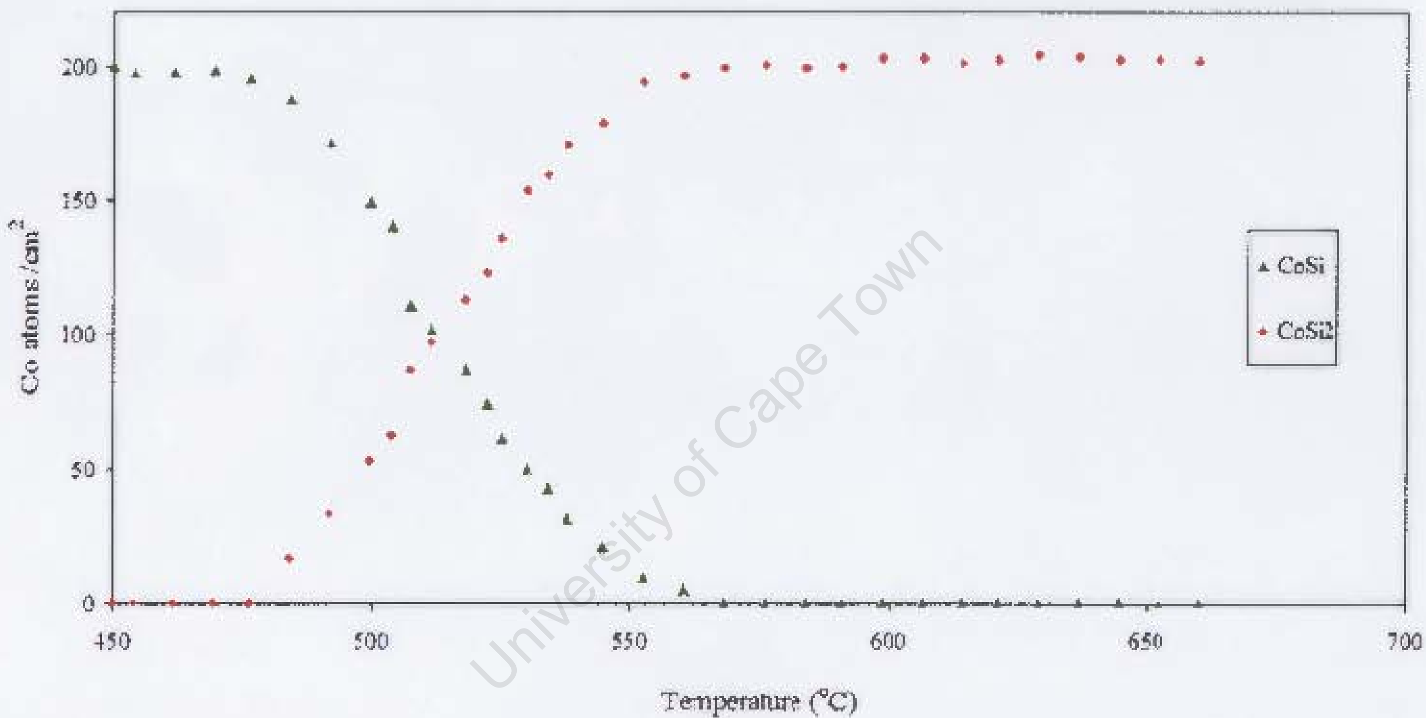

University of Cape Town

Figure A6: Results of the analysis of RBS spectra obtained form CoSi prepared by reactive deposition at 475 °C. The formation of $CoSi_2$ from CoSi started at calibrated temperature of 485 °C.

The formation of $CoSi_2$ from CoSi film prepared by reactive deposition at 525 °C

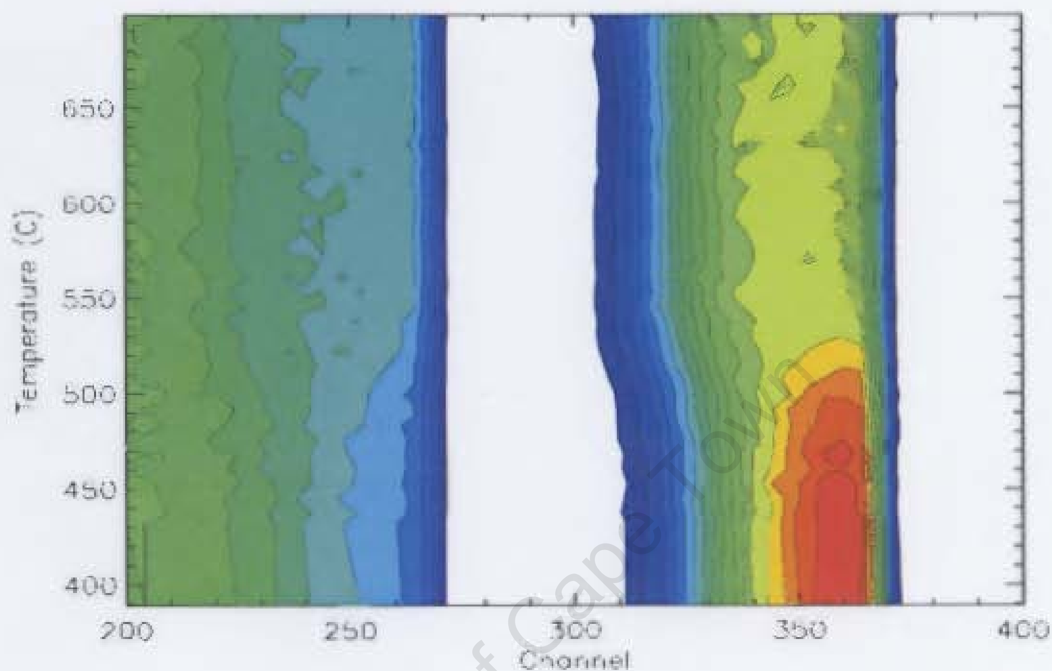

Figure A7: Contour plot of RBS data obtained during a ramped anneal (2 °C/min) of CoSi film prepared by reactive deposition at 525 °C.

University of Cape Town

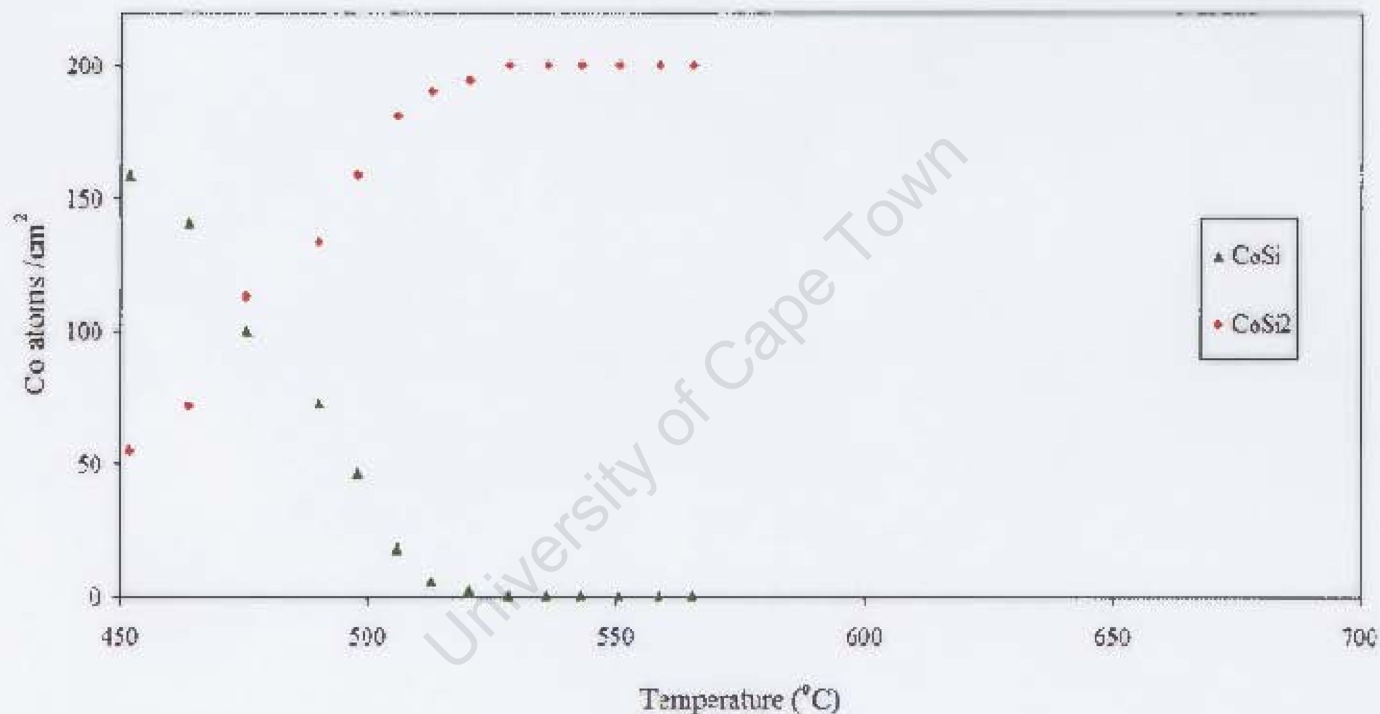

Figure A8: Results of the analysis of RBS spectra obtained form CoSi prepared by reactive deposition at 525 °C. The formation of $CoSi_2$ from CoSi initiated at calibrated temperature of 450 °C.

University of Cape Town

Appendix B

The XRD data obtained during ramped anneal at 1 °C/s of CoSi prepared by reactive depostion at 375 °C, 425 °C, 475 °C and 525 °C

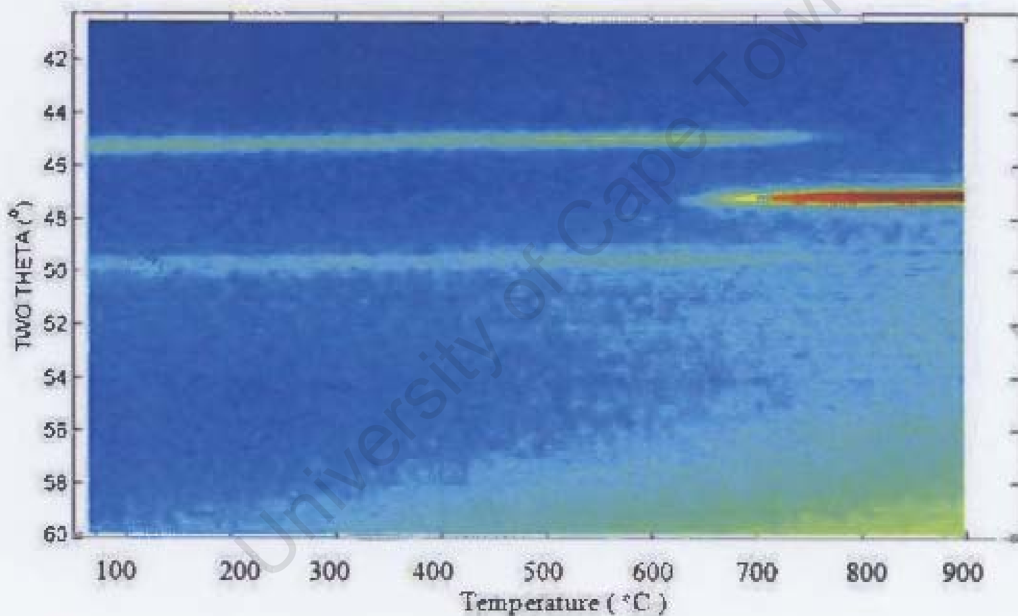

Figure B1: The XRD data obtained during the ramp annealing of CoSi prepared by reactive deposition at 375 °C (measurements of XRD data performed by J. Demeulemeester at Gent University).

University of Cape Town

Appendix B

The XRD data obtained during ramped anneal at 1 °C/s of CoSi prepared by reactive depostion at 375 °C, 425 °C, 475 °C and 525 °C

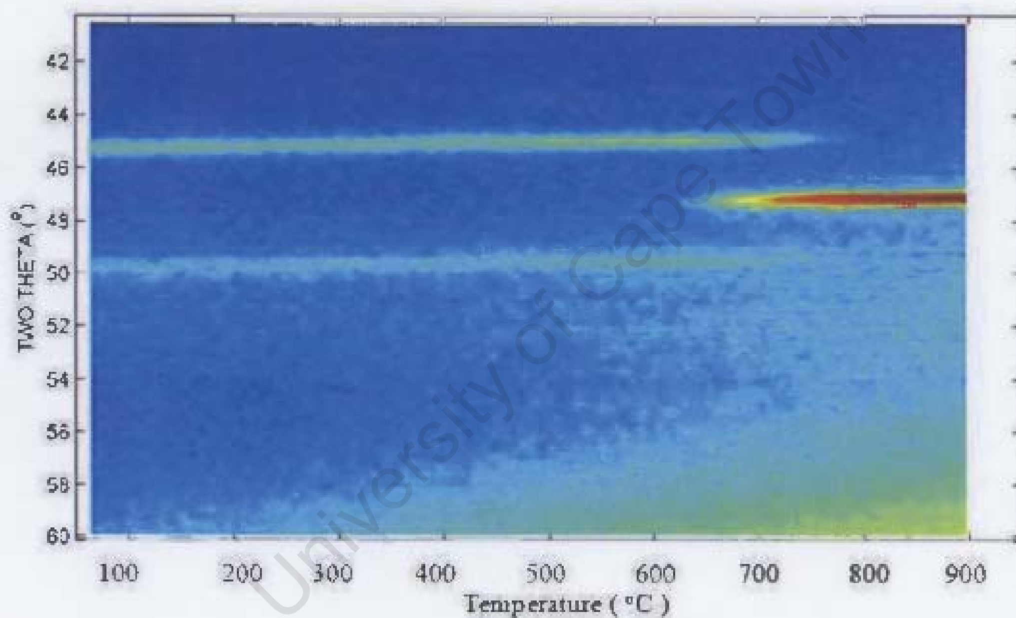

Figure B1: The XRD data obtained during the ramp annealing of CoSi prepared by reactive deposition at 375 °C (measurements of XRD data performed by J. Demeulemeester at Gent University).

University of Cape Town

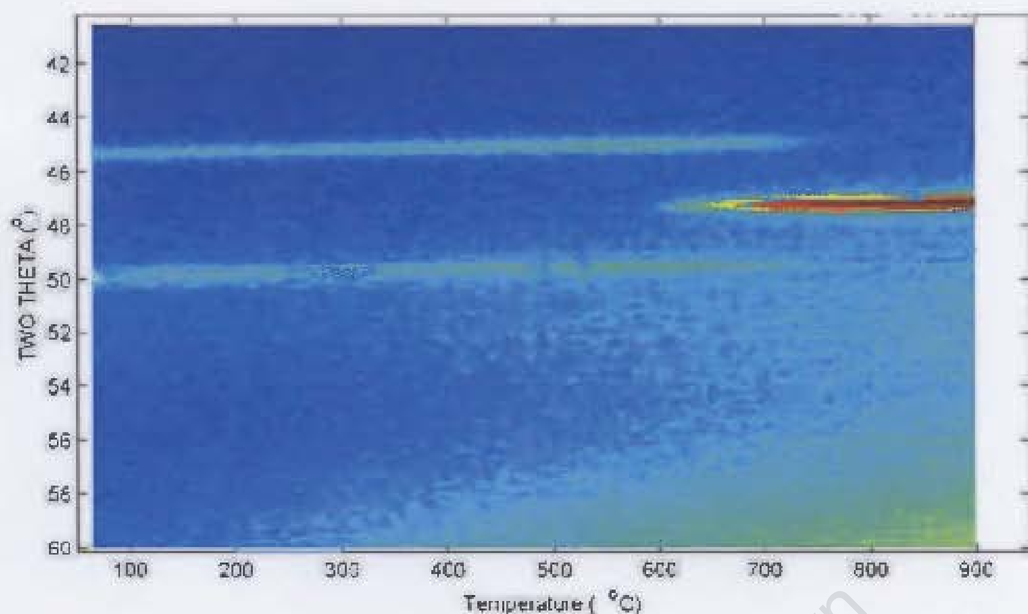

Figure B2: The XRD data obtained during the ramp annealing of CoSi prepared by reactive deposition at 425 °C (measurements of XRD data performed by J. Demeulemeester at Gent University).

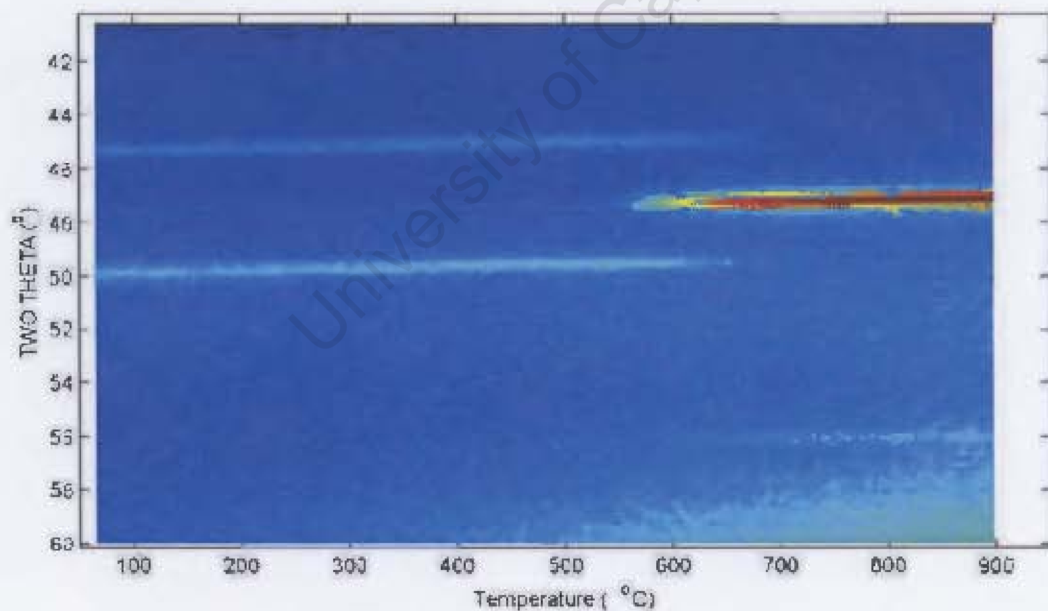

Figure B3: The XRD data obtained during the ramp annealing of CoSi prepared by reactive deposition at 475 °C (measurements of XRD data performed by J. Demeulemeester at Gent University).

University of Cape Town

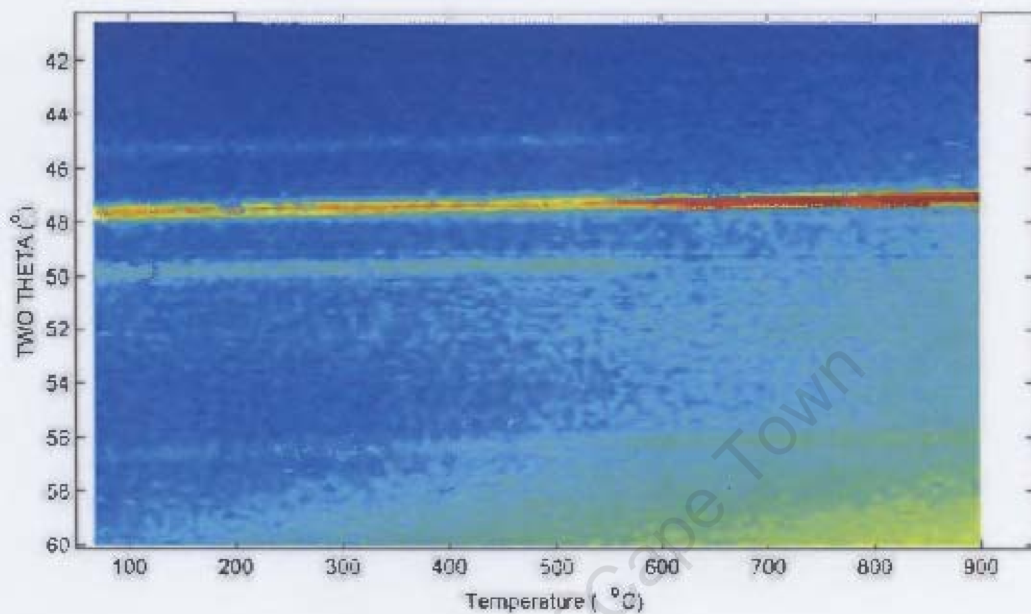

Figure B4: The XRD data obtained during the ramp annealing of CoSi prepared by reactive deposition at 525 °C (measurements of XRD data performed by J. Demeulemeester at Gent University).

University of Cape Town

Bibliography

Alberti, A., Bongiorno, C., Via, F. L. & Spinella, C. (2003), 'High-resolution investigation of atomic interdiffusion during co/ni/si phase transition', *Journal of Applied Physics* **94**, 231–237.

Appelbaum, A., Knoell, R. V. & Muraka, S. P. (1985), 'Study of cobalt-silicide formation from cobalt monosilicide', *Journal of Applied Physics* **57**(5), 1880–1886.

Barradas, N. P., Arstila, K., Battistig, G., Bianconi, M., Dytlewski, N., Jeynes, C., Kotai, E., Lulli, G., Mayer, M., Rauhala, E., Szilagyi, E. & Thompson, M. (2007), 'International atomic energy agency intercomparison of ion beam analysis software', *Nuclear Instruments and Methods in Physics Research* **262**, 281–303.

Bulle-Lieuwma, C. W. T. (1993), 'Epitaxial growth of $CoSi_2$/Si structures: A review', *Appllied Surface Science* **68**, 1–18.

Cahoon, E. C., Comrie, C. M. & Pretorius, R. (1984), 'Stability of $NiSi_2$ and $CoSi_2$ in contact with their free metal', *Applied Physics Letters* **44**.

Chamirian, O., Lauwers, A., Demeurisse, C., Guerault, H. & Vantomme, A. (2002), '$CoSi_2$ formation $Co_x\ ni_{1-x}$/ti system', *Microelectronic Engineering* **64**, 173–180.

Chen, C. J. & Waston, T. J. (1999), *Introduction to scanning tunnelling microscopy*, Oxford University Press, New York.

Chen, L. J. (2005), 'Metal silicides: An integral part of microelectronics', *JOM* **57**, 24–31.

Christain, J. W. (1975), *The theory of transformation in metals and alloys. PART 1: Equilibrium and general kinetic theory*, Pergamon Press, Oxford.

University of Cape Town

Chu, W. K., Mayer, J. W. & Nicolet, M. A. (1978), *Backscattering spectrometry*, Academic Press, New York.

Chu, W. K., Mayer, J. W., Nicolet, M. A., Buck, T. M., Amsel, G. & Eisen, F. (1973), 'Principles and applications of ion beam techniques for the analysis of solids and thin films', *Thin solid films,* **17**, 1–41.

Colgan, E. G., Jr, C. C. & Kotecki, D. E. (1995), 'Activation energy for CoSi and $CoSi_2$ formation measured during rapid thermal annealing', *Journal of Applied Physics* **77**, 614–619.

Comrie, C. M. (1996), 'Diffusing species and growth interfaces during cobalt disilicide formation', *Nuclear Instruments and Methods in Physics Research B* **118**, 119–122.

Comrie, C. M., Ahmed, H., Theron, C. C., Smeets, D., Demeulemeester, J., Vantomme, A. & Detavernier, C. (2007), 'Real-time rbs / xrd study of $CoSi_2$ formation from CoSi grown by reactive deposition', *Nuclear Instruments and Methods in Physics Research B* .

Comrie, C. M. & Egan, J. M. (1988), 'Diffusion of silicon in Pd_2Si during silicide formation', *Journal of Applied Physics* **64**.

Comrie, C. M., Egan, J. M., Liu, J. C. & Mayer, J. W. (1988), 'An investigation into the mechanism of epitaxial Pd_2Si formation', *South Africa Journal Of Science.* **84**.

Comrie, C. M., Falepin, A., Richard, O., Bender, H. & Vantomme, A. (2004), 'Metastable iron silicide phase formation by pulsed laser annealing', *Journal of Applied Physics* **95**.

Comrie, C. M. & Hoffman, V. (1993), 'Epitaxial cobalt disilicide formation by pulsed laser annealing', *South Africa Journal of Physics* **16**, 171–174.

Comrie, C. M. & Mcleod, J. E. (1992), 'Diffusion in cobalt silicide during silicide formation', *Crucial issues in semicondoctor materials and processing technologies, eds. S. Coffa, F. Priolo, E. Rimini and J.M. Poate (Kluwer, Dordrecht)* pp. 369–375.

Detavernier, C., Meirhaeghe, R. L. V. & Cardon, F. (2000), 'Influence of mixing entropy on nucleation of $CoSi_2$', *Physical Review B* **62**.

University of Cape Town

d'Heurle, F. M. (1988), 'Nucleation of a new phase from the interaction of two adjacent phases: some silicides', *Journal of Material Research* **3**, 167–195.

d'Heurle, F. M., Anflteatro, D. D., Deline, V. R. & Finstad, T. G. (1985), 'Reaction of silicon with films of co-ni alloys: phase separation of the monosilisides and nucleation of the disilicides', *Thin Solid Films,* **128**, 107–124.

d'Heurle, F. M. & Gas, P. (1986), 'Kinetics of formation of silicides: A review', *Journal of Material Research* **1**.

d'Heurle, F. M. & Petersson, C. (1985), 'Formation of thin films of $CoSi_2$: nucleation and diffusion mechanisms', *Thin Solid Films.* **128**, 283–297.

Doolittle, L. R. (1985), 'Algorithms for the rapid simulation of rutherford backscattering spectra', *Nuclear Instruments and Methods in Physics Research B* **9**(2), 344–351.

Doolittle, L. R. (1986), 'A semiautomatic algorithm for rutherford backscattering analysis', *Nuclear Instruments and Methods in Physics Research B* **15**(1), 227–231.

Falepin, A., Comrie, C. M., Vantomme, A. & Langouche, G. (2001), 'Study of phase formation in $\epsilon -$ FeSi layers by pulsed laser annealing', *Hyperfine Interactions* **134**(6), 153–160.

Falepin, A., Cottenier, S., Comrie, C. M., Richard, O., Bender, H., Langouche, G. & Vantomme, A. (2003), 'Formation and microstructure of cubic metastable iron silicides synthesized during pulses laser annealing', *Hyperfine interactions* **151/152**, 131–144.

Feldman, L. C. & Mayer, J. W. (1986), *Fundamentals of surface and thin film analysis*, North-Holland, New York.

Geiger, H. & Marsden, E. (1909), 'On a diffuse reflection of the α particles', *Royal Society* **82**, 495–500.

Glicksman, M. E. (2000), *Diffusion on solid*, Wiley, New York.

Gurp, G. J. & Langereis, C. (1975), 'Cobalt silicide layers on si structure and growth', *Journal of Applied Physics* **45**(5).

University of Cape Town

Jeon, H., Won, H., Kim, Y., Lee, J. & Nemanich, R. J. (2002), 'Analysis of ti-silicide formation with ta interlayer on si (100)', *Journal of the Korean Physical Society* **40**, 903–907.

Jeynes, C., Barradas, N. P., Marriott, P. K., Boudreault, G., Jenkin, M., Wendler, E. & Webb, R. P. (2003), 'Elemental thin film depth profiles by ion beam analysis using simulated annealing - a new tool', *Journal of Physics D: Applied Physics* **36**, 97–126.

Jimenez, J. R., Hsiung, L. M., Rajan, K., Schowalter, L. J., Hashimoto, S. & Thompson, R. D. (1990), 'Control of misoriented grains and pinholes in $CoSi_2$ grown on si(100)', *Applied Physics Letters* **57**(10), 2811–5030.

Kittl, J. A., Lauwers, A., Chamirian, O., van Dal, M., Akheyar, A., Potter, M. D., Lindsay, R. & Maex, K. (2003), 'Ni- and co-based silicides for advanced cmos applications', *Microelectronic Engineering* **70**(5), 158–165.

Klug, H. P. & Alexander, L. E. (1974), *X-ray Diffraction Procedures for polycrystalline and Amorphous Materials*, New York.

Kluth, P., Detavernier, C., Zhao, Q. T., Xu, J., Bochem, H. P., Lenk, S. & Mentl, S. (2000), 'Growth of patterned thin epitaxial $CoSi_2$ films by titanium oxide mediated epitaxy process', *Thin Solid Films* **380**, 201–203.

Lau, S. S., Mayer, J. W. & Tu, K. N. (1978), 'Interaction in co/si thin-film system kinetics', *Journal of Applied Physics* **49**.

Laurila, T. & Molarius, J. (2003), 'Reactive phase formation in thin film metal/metal and metal/silicon diffusion couples', *Crit. Rreviews in Sol. St. and Mat. Sc* **28**, 185–230.

Lauwers, A., Potter, M. D., Chamirian, O., Lindsay, R., Demeurisse, C., Vrancken, C. & Maex, K. (2002), 'Silicides for the 100-nm node and beyond: Co-silicide, co(ni)-silicide and ni-silicide', *Microelectronic Engineering* **64**(4), 131–142.

Lavoie, C., d'Heurle, F. M., Detavernier, C. & Jr, C. C. (2003), 'Towards implementation of a nickel silicide process for cmos technologies', *Microelectronic Engineering* **70**(3), 144–157.

University of Cape Town

Lien, C. D., Artur, M. & Nicolet, M. A. (1984), 'Marker experiments for the moving species in silicdies during solid phase epitaxy of evaporated Si', *Mat. Res. Soc. Symp. Proc.* **25**(6).

Lien, C. D., Nicolet, M. A. & Lau, S. S. (1984), 'Kinetics of $CoSi_2$ from evaporated silicon', *Applied Physics A* **34**(7), 249–251.

Lim, C. W., Petrov, I. & Greene, J. E. (2006), 'Epitaxial growth of $CoSi_2$ on Si(001) by reactive deposition epitaxy:island growth and coalescence', *Thin Silod Films* **515**, 1340–1348.

Magonov, S. & Whqugbo, M. T. (1996), *Surface analysis with STM and AFM: Experimental and theoretical aspects of image analysis*, VCH.

Mayer, M. (2008), 'Resolnra: A new program for optimizing the achievable depth resoluation of ion beam analysis methods', *Nuclear Instruments and Methods in Physics Research B* **266**, 1852–1857.

Mcleod, J. E., Wandt, M. A. E., Pretorius, R. & Comrie, C. M. (1992), 'Marker and radioactive silicon tracer studies of PtSi formation', *Journal of Applied Physics* **72**(1).

Mogul, H. C., Steck, A. J. & Novak, S. W. (1993), 'Shallow si ρ^+-n junctions fabricated by focused ion beam Ga^+ implantation through thin ti and $TiSi_2$ layers', *Journal of Applied Physics* **74**.

Molinder, G. (1956), 'A quantitative study of the formation of austenite and the solution of cementite at different austentitizing temperatures for 1.27 % carbon steel', *Acta Metallurgica* **4**, 565– 571.

Naidoo, R. Y., Comrie, C. M., Doyle, T. & Pertorius, R. (1993), 'High quality thin film superconductors formed in in situ by sputter deposition', *South African Journal of Physics* **16**.

Nicolet, M. A. & Lau, S. S. (1993), 'Formation and characterization of transition-metal silicides', *VLSI Electronics: Microstructure Science* **6**, 329–464.

Okamoto, H. & Massalski, T. B. (1983), 'The au-si (gold-silicon) system', *Bulletin of Alloy Phase Diagrams* **4**.

University of Cape Town

Ottaviani, G., Tu, K. N., Psaras, P. & Nobili, C. (1987), 'In situ resistivity measurement of cobalt silicide formation', *Journal of Applied Physics* **62**(1), 2290–2294.

Pretorius, R., Chen, M. C. & Ras, H. A. (1985), '$CoSi_2$ growth kinetics, phase sequence and mechanism', *Materials Letters* **3**, 282–285.

Pretorius, R., Wandt, M. A. E., McLeod, J. E., Botha, A. P. & Comrie, C. M. (1989), 'Determination of the diffusing species and diffusion mechanism during CoSi, nisi and ptsi formation by using radioactive silicon as a tracer', *Journal of the Electrochemical Society* **136**(26), 839–842.

Reader, A. H., W., J. P., Duchateau, B. & Crombeen, J. E. (1993), 'Epitaxial $CoSi_2$ formation on (001) Si by reactive deposition', *Semiconductor Science and Technology* **8**(8), 1204–1207.

Rennie, J., Elliott, S. R. & Jeynes, C. (1986), 'Rutherford backscattering study of the photodissolution of ag in amorphous $GeSe_2$', *Applied Physics Letters* **48**, 1430–1432.

Rutherford, E. (1911), 'The scattering of α and β particles by matter and the structure of the atom', *Philosophical Magazine* **21**, 669–688.

Smeets, D. (2007), Nucleation, diffusion and texture during growth of coni-silicides. Ph.D. Thesis, KU Leuven, Belgium.

Smoluchowski, R. (1952), 'Theory of grain boundary diffusion', *Physical Review* **87**.

Sweet, J. L. J. (2000), 'Synchrotron x-ray scattering techniques for microelectronics-related materials studies', *IBM J. Res. Develop* **44**, 457–476.

Theron, C. C. (1994), The influence of oxygen on the solid-state reaction between nickel and silicon. Masters Thesis, University of Stellenbosch, South Africa.

Theron, C. C. (1997), In situ, real-time characterization of solid state reaction in thin films. Ph.D. Thesis, University of Stellenbosch, South Africa.

Theron, C. C., Mars, J. A., Churms, C. L., Farmer, J. & Pretorius, R. (1998), 'In situ, real-time rbs measurement of solid state reaction in thin films', *Nuclear Instruments and Methods in Physics Research* **139**, 213–218.

University of Cape Town

Tung, R. T. (1992), 'Epitaxial $CoSi_2$ and $NiSi_2$ thin films', *Material Chemistry and Physics* **32**, 107–133.

van Dal, M. J. H., Huibers, D. G. G. M., Kodentsov, A. A. & van Loo, F. J. J. (2001), 'Formation of co-si intermetallics in bulk diffusion couples. part i. growth kinetics and mobilities of species in the silicide phases', *Intermetallics* **9**, 409–421.

Van, G. J., Weg, W. F. V. D. & Sigurd, D. (1978), 'Interaction in the co/si thin film system. diffusion-marker experiments', *Journal of Applied Physics* **45**(7).

Vantomme, A., Degroote, S., Dekoster, J., Bender, H. & Langouche, G. (1996), 'Effects of growth parameters on epitaxy of $CoSi_2$(100) formation by reactive deposition epitaxy', *Mater. Res. Soc. Symp. Proc.* **402**(3).

Vantomme, A., Degroote, S., Dekoster, J. & Langouche, G. (1995), 'Epitaxy of $CoSi_2$/si(100): from co/ti/si(100)', *Applied Surface Science* **91**(3), 24–29.

Vantomme, A., Nicolet, M. A. & Theodore, N. D. (1994), 'Epitaxial $CoSi_2$ films on si(100) by solid-phase reaction', *Journal of Applied Physics* **75**, 3882–3891.

Venables, J. A., Spiller, G. D. T. & Hanbucken, M. (1984), 'Nucleation and growth of thin films', *Reports on Progress in Physics* **47**, 399–459.

Walton, A. J. (1982), *Three phases of matter*, second edn, Oxford.

Wandt, M. A. E., Comrie, C. M., Mecleod, J. E. & Pertorius, R. (1990), 'Pt_2Si formation: diffusion marker and radioactive silicon tracer studies', *Journal of Applied Physics* **67**.

Wiesendanger, R. (1994), *Scanning probe microscopy and spectroscopy: Methods and applications*, Cambridge University Press.

Yalisove, S. M., Tung, R. T. & Loretto, D. (1989), 'Epitaxial orientation and morphology of thin $CoSi_2$ films grown on si(100): Effects of growth parameters', *Journal of Vacuum Science and Technology A* **7**, 1472–1474.

Ziegler, J. F. (1975), *Material analysis by nuclear backscattering*, Prenum press, New York.

University of Cape Town

Zingu, E. C., Comrie, C. M. & Pretorius, R. (1983), 'The effect of interposed silicide thickness on grown rate inbilayer silicide thin-film structure: The si(111)/Pd_2Si/cr system', *Journal of Applied Physics* **54**(2).

University of Cape Town